U-TSS: A novel time series segmentation model based U-net applied to automatic detection of interference events in geomagnetic field data (#108116)

First submission

Guidance from your Editor

Please submit by 28 Nov 2024 for the benefit of the authors (and your token reward) .



Structure and Criteria

Please read the 'Structure and Criteria' page for guidance.



Raw data check

Review the raw data.



Image check

Check that figures and images have not been inappropriately manipulated.

If this article is published your review will be made public. You can choose whether to sign your review. If uploading a PDF please remove any identifiable information (if you want to remain anonymous).

Files

Download and review all files from the <u>materials page</u>.

15 Figure file(s)

3 Table file(s)

Structure and Criteria



Structure your review

The review form is divided into 5 sections. Please consider these when composing your review:

- 1. BASIC REPORTING
- 2. EXPERIMENTAL DESIGN
- 3. VALIDITY OF THE FINDINGS
- 4. General comments
- 5. Confidential notes to the editor
- You can also annotate this PDF and upload it as part of your review

When ready submit online.

Editorial Criteria

Use these criteria points to structure your review. The full detailed editorial criteria is on your guidance page.

BASIC REPORTING

- Clear, unambiguous, professional English language used throughout.
- Intro & background to show context.
 Literature well referenced & relevant.
- Structure conforms to <u>PeerJ standards</u>, discipline norm, or improved for clarity.
- Figures are relevant, high quality, well labelled & described.
- Raw data supplied (see <u>PeerJ policy</u>).

EXPERIMENTAL DESIGN

- Original primary research within Scope of the journal.
- Research question well defined, relevant & meaningful. It is stated how the research fills an identified knowledge gap.
- Rigorous investigation performed to a high technical & ethical standard.
- Methods described with sufficient detail & information to replicate.

VALIDITY OF THE FINDINGS

- Impact and novelty is not assessed.

 Meaningful replication encouraged where rationale & benefit to literature is clearly stated.
- All underlying data have been provided; they are robust, statistically sound, & controlled.



Conclusions are well stated, linked to original research question & limited to supporting results.

Standout reviewing tips



The best reviewers use these techniques

Т	p

Support criticisms with evidence from the text or from other sources

Give specific suggestions on how to improve the manuscript

Comment on language and grammar issues

Organize by importance of the issues, and number your points

Please provide constructive criticism, and avoid personal opinions

Comment on strengths (as well as weaknesses) of the manuscript

Example

Smith et al (J of Methodology, 2005, V3, pp 123) have shown that the analysis you use in Lines 241-250 is not the most appropriate for this situation. Please explain why you used this method.

Your introduction needs more detail. I suggest that you improve the description at lines 57-86 to provide more justification for your study (specifically, you should expand upon the knowledge gap being filled).

The English language should be improved to ensure that an international audience can clearly understand your text. Some examples where the language could be improved include lines 23, 77, 121, 128 – the current phrasing makes comprehension difficult. I suggest you have a colleague who is proficient in English and familiar with the subject matter review your manuscript, or contact a professional editing service.

- 1. Your most important issue
- 2. The next most important item
- 3. ...
- 4. The least important points

I thank you for providing the raw data, however your supplemental files need more descriptive metadata identifiers to be useful to future readers. Although your results are compelling, the data analysis should be improved in the following ways: AA, BB, CC

I commend the authors for their extensive data set, compiled over many years of detailed fieldwork. In addition, the manuscript is clearly written in professional, unambiguous language. If there is a weakness, it is in the statistical analysis (as I have noted above) which should be improved upon before Acceptance.

U-TSS: A novel time series segmentation model based U-net applied to automatic detection of interference events in geomagnetic field data

Weifeng Shan ^{1, 2}, Mengyu Wang ¹, Jinzhu Xia ¹, Jun Chen ^{Corresp., 3}, Qi Li ^{Corresp., 4}, Lili Xing ¹, Ruilei Zhang ¹, Maofa Wang ⁵, Suqin Zhang ⁴, Xiuxia Zhang ⁶

Corresponding Authors: Jun Chen, Qi Li

Email address: shanyejunjie@163.com, darcyli@163.com

With the development of Internet of Things (IoT) technology, the collection of sensor data has become a vital aspect of big data acquisition. Traditional time series analysis methods struggle with complex patterns and long-term dependencies, whereas deep learning technologies offer new solutions. This study introduces the U-TSS, a U-net-based sequence-to-sequence fully convolutional network, specifically designed for onedimensional time series segmentation tasks. U-TSS maps input sequences of arbitrary length to corresponding sequences of class labels across different temporal scales. This is achieved by implicitly classifying each individual time point in the input time series and then aggregating these classifications over varying intervals to form the final prediction. This enables precise segmentation at each time step, ensuring both global sequence awareness and accurate classification of complex time series data. We applied U-TSS to geomagnetic field observation data for the detection of high-voltage direct current (HVDC) interference events. In experiments, U-TSS achieved superior performance in detecting HVDC interference events, with accuracies of 99.42%, 94.61%, and 95.54% on the training, validation, and test sets, respectively, outperforming state-of-the-art models in accuracy, precision, recall, F1-score, and AUC. Our code can be accessed openly in the GitHub repository at https://github.com/wangmengyu1/U-TSS .

¹ School of Emergency Management, Institute of Disaster Prevention, Sanhe, China

² Hebei Key Laboratory of Resource and Environmental Disaster Mechanism and Risk Monitoring, Sanhe, Hebei, China

Earthquake Administration of Anhui Province, Hefei, China

⁴ China Earthquake Administration, Institute of Geophysics, Beijing, China

⁵ Guilin University of Electronic Technology, Guangxi Key Laboratory of Trusted Software, Guilin, China

⁶ Earthquake Administration of Jiangsu Province, Nanjing, China

1 U-TSS: A Novel Time Series Segmentation model based U-net 2 **Applied to Automatic Detection of Interference Events in** 3 Gι **Geomagnetic Field Data** Ye 4 5 6 Weifeng Shan^{1,2}, Mengyu Wang¹, Jinzhu Xia¹, Jun Chen^{3*}, Qi Li^{4*}, Lili Xing¹, Ruilei Zhang¹, 7 Maofa Wang⁵, Suqin Zhang⁴, Xiuxia Zhang⁶ 8 9 10 ¹ School of Emergency Management, Institute of Disaster Prevention, Sanhe 065201, China (shanweifeng@cidp.edu.cn, 21661146@st.cidp.edu.cn, 23661710@st.cidp.edu.cn, xinglili@cidp.edu.cn, 11 12 zrl@cidp.edu.cn) 13 ² Hebei Key Laboratory of Resource and Environmental Disaster Mechanism and Risk Monitoring, Sanhe 14 065201, China(shanweifeng@cidp.edu.cn) 15 ³ Earthquake Administration of Anhui Province, Hefei 230031, China(shanyejunjie@163.com) 16 ⁴ Institute of Geophysics, China Earthquake Administration, Beijing 100081, China(darcyli@163.com, 17 13521519246@163.com) 18 ⁵ Guangxi Key Laboratory of Trusted Software, Guilin University of Electronic Technology, Guilin 541004, 19 China(wangmaofa2008@guet.edu.cn) 20 ⁶ Earthquake Administration of Jiangsu Province, Nanjing 210014, China(jsdzj xxzhang@outlook.com) 21 22 Corresponding Author: 23 Jun Chen³ 24 No. 558, West Changjiang Road, Shushan District, Hefei City, Anhui Province, China 25 Email address: shanyejunjie@163.com 26 Qi Li4 27 No.5, South Road, Nationalities University, Haidian District, Beijing, China 28 darcyli@163.com 29 30 **Abstract:** With the development of Internet of Things (IoT) technology, the collection of sensor data has become a vital aspect of big data acquisition. Traditional time series analysis methods 31 struggle with complex patterns and long-term dependencies, whereas deep learning technologies 32 33 offer new solutions. This study introduces the U-TSS, a U-net-based sequence-to-sequence fully 34 convolutional network, specifically designed for one-dimensional time series segmentation tasks. 35 U-TSS maps input sequences of arbitrary length to corresponding sequences of class labels 36 across different temporal scales. This is achieved by implicitly classifying each individual time 37 point in the input time series and then aggregating these classifications over varying intervals to

form the final prediction. This enables precise segmentation at each time step, ensuring both

global sequence awareness and accurate classification of complex time series data. We applied

38

39

- 40 U-TSS to geomagnetic field observation data for the detection of high-voltage direct current
- 41 (HVDC) interference events. In experiments, U-TSS achieved superior performance in detecting
- 42 HVDC interference events, with accuracies of 99.42%, 94.61%, and 95.54% on the training,
- validation, and test sets, respectively, outperforming state-of-the-art models in accuracy.
- 44 precision, recall, F1-score, and AUC. Our code can be accessed openly in the GitHub repository
- 45 at https://github.com/wangmengyu1/U-TSS.
- 46 **Keywords**: Time series segmentation; U-net; Artificial intelligence; Geomagnetic field
- 47 observation data; High-voltage direct current interference event;

1. Introduction

48

49 50

51

52

53

54

55

56 57

58

59

60

61

62 63

64

65 66

67

68

69 70

71 72

73

74

75

76

77

78

79

As innovations in Internet of Things (IoT) technology advance, the scope and complexity of sensor data acquisition have grown, establishing it as a crucial aspect of big data technologies (Yin et al. 2020). An increasing number of devices and sensors can collect and transmit real-time data, typically in the form of time series (Silva et al. 2021). Time series data is widely applied across various fields, including finance, ecology, economics, neuroscience, and physics (Matias et al. 2021). In the era of big data, the growing volume of data has revealed significant limitations of traditional time series analysis methods in handling complex patterns and long-term dependencies. The advancement of deep learning technologies provides new solutions for time series analysis. By employing Convolutional Neural Network (CNN) and Recurrent Neural Network (RNN), deep learning models can automatically extract latent features from time series data and capture complex temporal patterns. A growing body of research suggests that deep learning methods consistently outperform traditional approaches in time series forecasting, time series segmentation (TSS), time series classification and anomaly detection tasks.

Time series segmentation involves partitioning data into non-overlapping, automatically labeled segments. The primary objective of time series segmentation is to identify and delineate change points or event boundaries within the time series. This facilitates the organization of similar or related data segments while isolating dissimilar segments. To enable deep learning models to perform effective time series segmentation, it is essential to first label the data. Much like image segmentation tasks, where pixel-wise annotations aid in learning, properly labeled data plays a crucial role in training deep learning models for time series segmentation. The methods for labeling time series segmentation can be primarily categorized into two approaches: sliding window labeling and dense labeling (Gaugel & Reichert 2023). Figure 1 illustrates the distinction between sliding window labeling and dense labeling. Sliding window labeling involves dividing the time series data into several fixed-length subsequences, each of which is assigned a label. Although this method has produced satisfactory results in many applications, the accuracy of label prediction may be limited by both the size of the time window and the step size, especially when the lengths of the subsequences vary. In contrast, the dense labeling method provides a precise approach to time series segmentation that does not rely on sliding windows. By assigning labels to each time step in the time series, this method offers more detailed classification information.

81

82

83 84

85

86

87

88 89

90

91 92

93

94

95

96

97

98

99

100101

102

103

104

105106

107

108

109110

111

112

113

114115

116

117

118119

Similar to semantic segmentation in computer vision, effective time series segmentation depends on dense labeling and robust model architectures to ensure precise classification. In dense labeling, each individual data point, whether part of a time series or an image pixel, is assigned a specific category. A pivotal architecture in semantic segmentation is the fully convolutional network (FCN) (Long et al. 2015), which has significantly contributed to end-to-end pixel-level predictions. Based on FCN, many advanced convolutional neural networks have been proposed, including U-net (Ronneberger et al. 2015), which has been widely used in various segmentation tasks. U-net's symmetric contracting and expanding paths form a U-shape, and the network uses skip connections to combine positional and semantic information. Segnet (Badrinarayanan et al. 2017) is similar to the U-net network, but it uses indexing for up-sampling to better preserve the boundary feature information. Deeplab (Chen et al. 2017) used dilated convolution and fully connected conditional random fields to improve the segmentation accuracy for image segmentation. Recent research has shown that all of these methods have been quite successful in the field of image segmentation.

Despite the advancements in segmentation techniques for images data, the inherent complexity and unique characteristics of time series data in other fields necessitate specialized segmentation methods. For instance, sleep staging and human activity recognition (HAR) are two major areas of study within time series segmentation, offering a wealth of experimental results and research insights (Yu et al. 2019). Huy Phan et al. (Phan et al. 2019) introduced SeaSleepNet, a hierarchical RNN designed for sleep staging, which enables end-to-end training of the network and classifies each time step of the time series to generate an output label sequence. Akara Supratak et al. (Supratak et al. 2017) developed DeepSleepNet, a model that employs CNN to extract temporal features and utilizes bidirectional long short-term memory networks (BiLSTM) to automatically learn the transition rules between sleep stages from electroencephalogram signals. Perslev Jensen (Perslev et al. 2019) proposed U-Time, a fully feed-forward deep learning algorithm for studying physiological time series segmentation of sleep data. U-Time classifies each time point in the input signal and aggregates them at fixed intervals to produce a final prediction. U-Sleep (Perslev et al. 2021) is an extension of U-Time designed for physiological time series segmentation applications, such as sleep staging. U-Sleep enables the marking of sleep stages at shorter intervals and facilitates automatic sleep staging. Yasin Kaya (Zhang et al. 2024) developed a deep learning method based on 1D-CNN for human activity recognition, evaluating the model using three public datasets, all of which yielded satisfactory results. Nidhi Dua (Dua et al. 2021) employed an end-to-end model for automatic feature extraction and activity classification. This model, which combines CNN and gated recurrent units (GRU), demonstrated robust classification performance across three publicly available human activity recognition datasets.

In the field of geomagnetism, geomagnetic field observation data provides robust support for enhancing earthquake prediction and advancing research on seismomagnetic relationships. For earthquake prediction, large-scale geomagnetic observation instruments generate substantial volumes of time series data, capturing the state of the geomagnetic field over time (Chen et al.

121

122

123 124

125

126

127

128

129

130

131 132

133

134

135

136

137

138

139

140 141

142

143

144

145 146

147

148

149 150

151

152

153

154

155

156

2016: Zhang et al. 2016). As modern infrastructure expands, various sources of interference. including highways, subways, and high-voltage direct current (HVDC) transmission lines, have introduced significant undesired noise into geomagnetic data collection (Shen et al. 2005). If these interference events are not detected and preprocessed, geomagnetic field observation data cannot be applied to earthquake forecasting and seismomagnetic relationship research (Chen et al. 2008; Lin et al. 2020). Among various interference events, HVDC interference events have a wide range of impacts and high frequency. When HVDC transmission lines are powered on or experience faults, unbalanced currents on the two high-voltage lines generate an uncompensated magnetic field, thereby affecting the geomagnetic field observation data (Gong & Yu 2000; Jiang & XiuXia 2014), as shown in Fig. 2. Because of the unequal magnitudes of unbalanced currents on the two HVDC transmission lines and the varying distances between the geomagnetic observation instruments and HVDC transmission lines, HVDC interference events exhibit staircase-like characteristics in the Z-component of the geomagnetic field observation data, with varying durations, amplitudes, and orientations, while showing less pronounced effects on the other observation components. The variability further complicates the time series analysis and accurate detection of interference events. HVDC interference events have become a focal point in the preprocessing of geomagnetic field observation data (Chen et al. 2010). Existing manual detection methods are not only time-consuming and labor-intensive, but also highly susceptible to human variability, with results differing significantly between individuals. This inconsistency leads to a lack of uniformity in data processing outcomes, reducing the reliability and overall quality of the processed geomagnetic field data. Therefore, there is an urgent need for a highlyaccurate and universally applicable automatic detection method for HVDC interference events.

In contrast to sleep staging and human activity recognition, the primary challenge in geomagnetic field observation data preprocessing is the precise detection of interference events. For earthquake prediction, accurately identifying and process these interference events is critical, as even minor errors in detection can significantly compromise the reliability of the data. To address these challenges, this study draws inspiration from advancements in time series segmentation and semantic segmentation and proposes a sequence-to-sequence time series segmentation model based on U-net. We apply this model to the detection of HVDC interference events in geomagnetic field observation data, enabling the segmentation of the entire time series and the identification of HVDC interference events of varying durations at any temporal scale. The key contributions of this study are as follows:

- We proposed U-TSS, a novel time series segmentation model based on U-net. This model combines time series segmentation techniques with semantic segmentation to achieve highprecision dense segmentation of interference events in geomagnetic field observation data. This innovative integration effectively leverages the advantages of the U-net architecture. thereby enhancing the ability to capture complex temporal features and patterns.
- The model employs a sequence-to-sequence framework, utilizing one day's geomagnetic 157 field observation data as input. It implicitly classifies each individual time point in the input 158 159 data and aggregates these classifications into time series segments of varying lengths to

- produce the final predictions. This design enables the model to accurately classify each time step, significantly improving the accuracy and robustness of the dense segmentation.
 - By employing the Particle Swarm Optimization (PSO) algorithm (Kennedy & Eberhart 1995) to optimize the model's hyperparameters, the model's performance is further enhanced. The introduction of the PSO algorithm not only accelerates the model's convergence speed but also optimizes the selection of hyperparameters, allowing U-TSS to demonstrate higher efficiency and accuracy when processing geomagnetic field observation data.

In the remainder of the paper, we outline the overall structure. Section 2 formalizes the problem.

Section 3 provides an overview of the U-TSS architecture and its modules. Section 4 details the data sources and the sample production process. Section 5 presents a series of tests conducted with state-of-the-art time series segmentation models. Section 6 describes the results of the experiment. Section 7 makes a discussion, and Section 8 concludes this essay.

2. Problem formalization

U-TSS is a sequence-to-sequence fully convolutional network designed specifically for onedimensional time series segmentation tasks. Built upon the U-Net architecture, this model effectively addresses the limitations of traditional segmentation models when handling complex time series data. U-TSS processes time series data of arbitrary length as input, efficiently mapping the complete sequence to dense outputs in a single forward pass using fully convolutional layers. This design enhances the model's capacity to capture global patterns in long sequences while ensuring precise segmentation at each time step, enabling accurate classification of complex temporal signals.

The problem of time series segmentation can be formally defined as follows: Let $X_C \in \mathbb{R}^{T \times C} = [X_1, X_2, \cdots, X_C]$ represent the multivariate time series data for a specific time interval, where T denotes the number of time steps and C represents the different features of the time series data. In this study, we focus on a univariate case, thus C = 1. Consequently, the univariate time series data can be expressed as a one-dimensional array $X \in \mathbb{R}^{T \times 1} = [x_1, x_2, \cdots, x_T]$. To address the segmentation problem, each time step T is associated with a label $Y_T \in \mathbb{R}^{T \times 1}$, which indicates the category to which the time step belongs. This labeling approach constitutes a dense annotation method, which is essential for the segmentation task, as it enables the precise categorization of each time point according to its respective class.

In the context of geomagnetic field observation data, the input data X for the U-TSS model consists of one-dimensional time series data with the shape $R^{T \times 1}$, corresponding to the measurements of a specific component across T time steps. The primary task is to map this input data to a sequence of predicted labels $\hat{Y}_T \in R^{T \times 1}$, producing an output for each time step. The objective is to accurately identify and localize HVDC interference events in the geomagnetic observation data, resulting in a label sequence where HVDC events are marked as 1 and the BACKGROUND is marked as 0.

This flexibility in assigning labels to every time point is a key feature of U-TSS, allowing it to handle fine-grained temporal segmentation tasks effectively. U-TSS implicitly classifies each time point in the input data and aggregates these classifications into time series segments of varying lengths. This approach enables the accurate detection of HVDC interference events in geomagnetic field observation data, thereby enhancing the accuracy and efficiency of time series segmentation methods.

3. Method

3.1 U-TSS Model Overview

To achieve the precise detection of HVDC interference events in geomagnetic field observation data, U-TSS is an adaptation of the U-Net model, originally designed for biomedical image segmentation. The U-Net model is structured with both a contracting path and an expanding path, enabling effective feature extraction and reconstruction. As illustrated in Fig. 3 the left side of the network represents the contracting path, comprising four contraction stages. Each contraction stage includes two 3×3 convolutional layers and one 2×2 max pooling layer. After each contraction stage, the number of feature maps doubles while the feature maps are halved in size. The expanding path is located on the right side of the network structure and is made up of four stages. Each expansion stage includes one 2×2 Up-convolutional layer and two 3×3 convolutional layers. The number of feature maps is reduced by half through deconvolution, and then connected to the symmetric feature maps from the contracting path on the left side. Because of the difference in size between the contracting and expanding path feature maps, the U-Net model crops the contracting path feature maps to match the size of the symmetric feature maps on the right side. The final output is obtained by applying a 1×1 convolutional layer to the entire model.

Figure 4 illustrates the network structure of the U-TSS model, comprising three primary modules: the contracting path, the expanding path, and a dense segmentation classifier. The contracting path focuses on feature extraction by progressively down-sampling the input time series. It captures relevant temporal patterns through convolutional operations and reduces the temporal resolution via pooling layers. The expanding path is designed to up-sampling the feature maps obtained from the contracting path, restoring the original resolution of the input. By incorporating skip connections, the model combines coarse and high-level features with fine details, which enhances its capacity for accurate time series segmentation. The dense segmentation classifier assigns a label to each time step of the input sequence. It leverages the outputs from the expanding path to produce a dense output, generating class probabilities for every time step in the time series. The design of these three modules enables the U-TSS model to effectively achieve precise segmentation and classification of time series.

The U-TSS model modifies the conventional U-Net architecture, which was originally developed for two-dimensional image data, to effectively accommodate one-dimensional time series data. Specifically, the U-TSS employs 1-dimensional convolutions to effectively extract features related to HVDC interference events in geomagnetic field observation data. In contrast to 2-dimensional convolution, where a sliding window operates over the feature map in both

width and height directions, the 1-dimensional convolution focuses solely on the width direction. 238 This approach allows for efficient processing of the time series data, as it multiplies and sums 239 values at corresponding positions within a single dimension. The mechanics of 1-dimensional 240 convolution are illustrated in Fig. 5. To ensure that the input feature maps of the convolution 241 242 process are consistent with the output feature maps and to avoid the cropping operation during feature fusion, the U-TSS model uses SAME convolution. The convolution kernel size in Fig. 5 243 is three and it moves across the input sequence in fixed steps. At each step, the convolution 244 kernel computes the output value by multiplying and summing the elements corresponding to its 245 current position in the input region. Afterwards, the convolution kernel shifts by one step, 246 repeating this operation until the entire input sequence is traversed. Each convolution calculation 247 produces a point in the output feature map, resulting in a new feature map after the convolution 248 process. Assuming that n is the current convolutional layer, the 1-dimensional convolutional 249 operation formula for this layer is shown in Eq. (1): 250

$$Q_j^n = \sum_{i=1}^K Q_{j+i-1}^{n-1} \times W_{ij}^n + b_j^n$$
 (1)

Where Q_j^n represents the output at the position j after the n-th convolutional layer, K is the size of the convolutional kernel, i is the convolution kernel index, and j represents the position index in the output feature map of the n-th layer. \times denotes the convolutional operation, W_{ij}^n represents the weight of the convolution kernel at the i-th position for the j-th output in the n-th layer, and b_j^n is the bias corresponding to the output features at position j in layer n.

Following the convolution operation, each output value is often transformed nonlinearly by using an activation function in order to improve the network model's non-linear features. The activation function used in U-TSS is ReLu, which can be represented as Eq. (2):

$$y_{j}^{n} = f(Q_{j}^{n}) = \max\{0, Q_{j}^{n}\} = \begin{cases} Q_{j}^{n}, & Q_{j}^{n} \ge 0\\ 0, & Q_{j}^{n} < 0 \end{cases}$$
 (2)

Where Q_j^n represents the input value at location j to the activation function from the convolution operation, y_j^n denotes the output value at location j after the activation function is applied in the n-th layer.

3.2 Contracting path

251

252

253

254

255

256257

258

259

260

261

262

263

264265

266

267268

269

270

271

The contracting path consists of four stages, each including a max pooling layer with a pooling size of 2 and two 1-dimensional convolutional layers. Max pooling preserves the most salient features by selecting the maximum value in a local region as the output value. Figure 6 illustrates the max pooling process. The pooling window in the figure is 2, moving in steps of 2 across the inputs and selecting the maximum value to pass to the next layer. Additionally, dropout layers are applied to the first and second convolutional layers in the first two contraction stages. With each contraction stage, the number of feature maps doubles while the feature maps are halved in size. The contracting path continuously performs convolution and pooling operations to obtain deep semantic information. As the data are pooled several times, the

resulting low-resolution feature maps reflect the time-point semantic information, that is, each individual time-point of the geomagnetic field observation data is assigned a label.

3.3 Expanding path

In the expanding path, there are four expansion stages, each involving an up-sampling operation with a factor of 2, followed by two 1-dimensional convolutional layers. In the first expansion stage, a dropout layer is introduced between the two convolutional layers. Similarly, in the third and fourth expansion stages, a dropout layer is added to each of the two 1-dimensional convolutional layers. After four expansion stages, the feature maps are equal in size to the input. Throughout the continuous up-sampling process, the network can obtain deep feature information about the data. In each expansion stage, the high-resolution features of the contracting path are transferred and mixed with the up-sampled features, resulting in a doubling of the feature maps, which is the skip connection. Subsequent convolutions are then performed to capture contextual information in the encoded representations. The skip connection helps the model to successfully fuse deep semantic information with shallow positional information, achieve effective fusion of multi-scale HVDC interference events and overcome the issues of positional loss and segmentation inaccuracy in the segmentation process.

3.4 Dense segmentation classifier

The final module of the U-TSS model is the dense segmentation classifier, which assigns a label to each time step in the input sequence. Utilizing the output of the expanding path, this head constructs a probability distribution over the classes using softmax activation. This process results in the final predictions $\hat{Y} \in R^{T \times 1}$, where T represents the number of time steps. By constructing this probability distribution, the dense segmentation classifier quantifies the likelihood that each observed value in the input data corresponds to an HVDC event or the BACKGROUND. This mechanism not only ensures dense segmentation by providing a label for each time step but also aggregates these classifications into segments of varying lengths, thereby allowing the U-TSS model to accurately detect HVDC interference events in the geomagnetic field observation data and pinpoint the start and end times of these events.

4. Dataset

4.1 Data Source

The data used in this dy were obtained from the Geomagnetic Network Center of China, the Institute of Geophysics, China Earthquake Administration. In this paper, the geomagnetic field observation data and manual preprocessing logs of HVDC interference events between January 1, 2014, and December 31, 2018, were selected for the experiments. The manual preprocessing log of HVDC interference events contains the station code, instrument code, item code, and the start and end time of each HVDC event. Each station may deploy multiple geomagnetic instruments. The HVDC interference events mainly affect the Z-component of the geomagnetic field observation data, characterized by a step-like pattern (Bao et al. 2020; Yang & Dong 2020). Therefore, in this study, we used the Z-component of the geomagnetic field

4.2 HVDC sample production

observation data to detect HVDC interference events automatically.

 The detection of HVDC interference events has primarily relied on manual inspection methods, which are often characterized by substantial time requirements and a susceptibility to human error. Furthermore, the absence of a standardized dataset for these events presents significant challenges for the advancement and validation of automated detection algorithms. Consequently, we produced a dataset specifically for the detection of HVDC interference events in geomagnetic field observation data. In this subsection, we describe the process of sample production in detail. Figure 7 illustrates the sample production process.

Firstly, we selected all HVDC interference events from January 1, 2014, to December 31, 2018, from the manual preprocessing log and recorded the date, start time, end time, and affected instrument of each HVDC event.

Before generating samples, we combined all HVDC events in one day for each instrument intering single record. The observation data is then normalized using the Z-score, formulated as:

$$Z_i = \frac{X_i - \mu}{\sigma} \tag{3}$$

where X_i is the raw observation at time i, μ is the mean of the observation data, and σ is the standard deviation. The normalized data is saved as a data file for the HVDC sample, named 'station_code-instrument_code-date .npy

Finally, similar to the sample generation method in semantic segmentation, the U-TSS model needs to label each time point value in the geomagnetic field observation time series sample as BACKGROUND or HVDC. If a time point value is an HVDC interference event, it is labeled as 1, otherwise, it is labeled as 0. After the above operation, we get a label file with the same name as the data file of the HVDC sample, which is stored in the label folder. Therefore, each HVDC sample contains one data file and one label file, and has a consistent length.

Figure 8 shows an HVDC sample from station 12005, instrument 1, on July 3, 2017. The top half of the figure shows geomagnetic field observation data after normalization. The black line represents the background, and the red line indicates the HVDC interference events that occurred on that day. The bottom half of the figure shows the labels corresponding to the data, where 1 indicates HVDC, and 0 indicates the background.

A total of 9255 samples were generated, covering 126 affected observation stations. To improve the generalization ability of the model, the 9255 samples were randomly shuffled and divided into three sets: 7405 samples for training, 925 samples for validation, and 925 samples for testing, in an 8:1:1 ratio.

5. Experiments

5.1 Experiment setting

The U-TSS model proposed in this paper was developed using Python with Keras for the model design and construction. TensorFlow was chosen as the underlying deep learning library (Abadi et al. 2016). Training the model employed two NVIDIA Tesla V100 FHHL 16G GPU cards, with two Intel(R) Xeon(R) Silver 4116 CPUs @ 2.10GHz processors and 256GB of memory. The Adam optimizer was used (Diederik & Ba 2014), with a batch size of 64 for the training set and a batch size of 2 for the validation set. The number of epochs was set to 300.

Throughout the training process, we incorporated the early stopping mechanism, monitoring the accuracy of the model on the validation set. The PATIENCE value was set to 20, meaning that if there was no consecutive improvement in the validation set accuracy over 20 epochs, training would be immediately halted. Each epoch took approximately 16 seconds to train.

The model aims to minimize the loss function $L(Y,\hat{Y})$, which represents the distance between the predicted labels \hat{Y} and the true labels Y. The categorical cross-entropy loss function was employed in this experiment to address the binary classification task, defined by the following formula:

$$L(Y,\hat{Y}) = -\frac{1}{n} \sum_{T=1}^{n} Y_T * \log(\hat{Y}_T)$$
 (4)

358 where \hat{Y}_T represents the predicted result of the sample and Y_T represents the true calculated 359 result.

5.2 Evaluation metrics

Whether a time point value is an HVDC interference event can be viewed as a binary classification problem. In this study, evaluation metrics were accuracy, precision, recall, F1-score, and AUC. Table 1 presents the confusion matrix for predicting whether a time point using the U-TSS model.

HVDC is considered as the positive class, while BACKGROUND is considered as the negative class. True positive (TP) and true negative (TN) represent correct predictions, where the true label value and the predicted label value are the same. False positive (FP) and false negative (FN) represent incorrect predictions, where the true label value and the predicted label value are different.

Accuracy is defined as the proportion of correctly classified samples, including both HVDC and BACKGROUND data, to the total number of samples. It is calculated using the Eq. (5).

$$accuracy = \frac{TP + TN}{TP + FP + TN + FN}.$$
 (5)

The precision is utilized to evaluate the model's accuracy in predicting HVDC samples, which is defined as the proportion of correctly predicted HVDC samples to the total predicted HVDC samples. It can be calculated using Eq. (6).

$$precision = \frac{TP}{TP + FP}.$$
 (6)

The recall, which is the percentage of samples predicted to be HVDC among all actual HVDC samples, is used to assess the model's capacity to identify HVDC samples. It is calculated using Eq. (7).

$$recall = \frac{TP}{TP + FN}. (7)$$

A harmonic mean of recall and precision is the F1-score. It gives a fair assessment by taking recall and precision into account. It is defined as shown in Eq. (8).

$$F1 - scrore = \frac{2 * precision * recall}{precision + recall}.$$
 (8)

381

382

383 384

385

386

387

388

389 390

391

392

393 394

395

396

397 398

399

400

401

402 403

404

405

406 407

408

409

410 411

412

413

414

The area under the receiver operating characteristic (ROC) curve, which is a plot of the true positive rate (TPR) against the false positive rate (FPR) for different threshold values, is referred to as the AUC (Area Under the Curve). AUC is utilized to evaluate a classifier's performance, particularly in situations with sample imbalance. The TPR and FPR are calculated as follows, according to Eq. (9) and Eq. (10).

$$TPRate = \frac{TP}{TP + FN} \tag{9}$$

$$FPRate = \frac{FP}{FP + TN} \tag{10}$$

5.3 Hyperparameter optimization

As the accuracy of deep learning models heavily relies on hyperparameters such as the learning rate and convolution kernel size, selecting the optimal values for these hyperparameters is a challenging task. Due to their straightforward logic structures, excellent optimization quality and efficiency, and low computational costs, numerous enhanced meta-heuristic techniques have been created in recent decades for resolving challenging optimization problems (Wang et al. 2023). In this paper, the primary hyperparameters of the U-TSS model were optimized using the particle swarm optimization algorithm. PSO is a stochastic search algorithm based on swarm collaboration, which was developed by simulating bird foraging behavior, and is now commonly used in hyperparameter optimization in deep learning models (Band et al. 2020; Elmasry et al. 2020; Qolomany et al. 2017). The learning rate, convolution kernel size_and dropout size were selected as the hyperparameters to be optimized, with the value of the 1 score set as the fitness function. In the PSO optimization algorithm, the hyperparameters to be optimized were continuously updated within the upper and lower bounds set, and the particle swarm iteratively searched for the minimum value of the fitness function, returning the final optimized results for all hyperparameters when this minimum value was achieved. In the optimization process, the lower and upper bounds of the convolution kernel size were set from 16 to 128, while the lower and upper bounds of the learning rate were set from 0.000001 to 0.01. The dropout sizes in the first and second compression stages of the compressed path, as well as the third and fourth expansion stages of the expansive path, were referred to as dropout₁. The dropout size in the first expansion stage of the expansive path was referred to as dropout₂. Both dropout₁ and dropout₂ were bounded within the range of 0 to 0.6. The parameter settings for PSO optimization of the hyperparameters experiment are presented in Table 2.

The values of the fitness function (1-F1-score) obtained at each ration in the optimization process are illustrated in Fig. 9. The x-axis represents the iteration number, and the y-axis represents the value of the fitness function (1-F1-score). It can be observed that the value of the fitness function gradually decreased with an increasing number of iterations and eventually reached stability. This indicates a progressive improvement of the F1-score of the U-TSS model during the optimization process. Ultimately, the optimal values of the hyperparameters are as

follows: the learning rate is 0.00005, the convolution kernel size is 64, and dropout₁ and dropout₂ are 0.1 and 0.4, respectively.

6. Results

417 418

419

420 421

422 423

424 425

426

427

428

429

430

431 432

433

434

435

436 437

438

439

440 441

442

443

444

445

446 447

448 449

450

451

452

453

454

The accuracy and loss curves of the U-TSS model are shown in Fig. 10. During the training process, the accuracy on both the training and validation sets gradually increased, eventually reaching 99.42% and 94.61%, respectively. The U-TSS model achieved 95.54% accuracy, 88.65% precision, 76.07% recall, and an F1-score of 0.8188 on the testing set.

To evaluate the performance of U-TSS, we selected several typical time series segmentation methods for comparison. Although there is limited literature specifically applying deep learning algorithms to detect HVDC interference events, we drew on the similarities between geomagnetic field observation data and time series data in biomedical fields, such as electrocardiogram (ECG) and electroencephalogram (EEG). Therefore, we compared U-TSS with several established segmentation algorithms commonly used in these fields, including the CNN (Acharva et al. 2017), CNN-LSTM (Oh et al. 2018), TinySleepNet (Supratak & Guo 2020), and U-Time models. In addition, considering that geomagnetic field observation data are classical time series data, we also included several traditional time series classification methods in our comparison. These methods encompass the Encoder model (Serra et al. 2018), FCN (Wang et al. 2017), ResNet, and Inception model (Ismail Fawaz et al. 2020). All models were trained and tested on the same datasets to assess their generalization ability. In the comparative experiments, all hyperparameters were configured based on the original papers of the aforementioned models. Consistent with the training approach of the U-TSS model, an early stopping mechanism was implemented with a maximum of 300 iterations and a patience of 20.

Table 3 presents comparative experimental results on the test set, illustrating that the U-TSS model achieves the best performance on all metrics, including accuracy 95.54%, precision 88.65%, recall rate 76.07%, F1-score 0.8188, and AUC 0.9637. In comparison, the first-order difference method achieves 73.04% accuracy, 24.29% precision, 48.78% recall, and 0.3243 F1score. It is unable to compute its AUC due to differing data input formats. The CNN model achieves an accuracy of 90.03%, with precision at 70.19%, recall at 43.13%, an F1-score of 0.5343, and an AUC of 0.8995. The CNN-LSTM model achieves 91.21% accuracy, 75.45% precision, 49.99% recall, an F1-score of 0.6013, and an AUC of 0.7405. The TinySleepNet model achieves 90.11% accuracy, 83.98% precision, 68.00% recall, and an F1-score of 0.7257. The TinySleepNet could not calculate its AUC due to data format issues. The U-Time model achieves 86.22% accuracy, 29.52% precision, 32.99% recall, an F1-score of 0.3116, and an ALIC of 0.7130. The Encoder model achieves 87.99% accuracy, 85.71% precision, 11.37% recall, and F1-score of 0.2007, and an AUC of 0.4870. The FCN model achieves 86.74% accuracy, 63.06% precision, 0.14% recall, an F1-score of 0.0027, and an AUC of 0.6706. The Inception model achieves 85.03% accuracy, 23.91% precision, 5.90% recall, an F1-score of 0.0946, and an AUC of 0.3968. The Resnet model achieves 86.76% accuracy, 56.67% precision, 0.90% recall, F1score of 0.0177, and AUC of 0.8985.

The results from the experiment indicate that the proposed U-TSS model achieves the highest scores across all evaluation metrics, demonstrating superior overall performance. It surpasses both traditional statistical methods and state-of-the-art deep learning approaches in detecting HVDC interference events.

Figure 11 depicts the ROC curves for all models except the first-order difference method and the TinySleepNet model. The AUC in the figure represents the performance metric, where a larger area indicates better model performance. From the figure, it is evident that the U-T exhibits the highest performance.

Figure 12 illustrates the detection results of various models for HVDC interference events on geomagnetic observation data recorded on May 7, 2023, from station code 14014 and instrument code 1. The U-TSS model excels in both detection accuracy and overall precision compared to other models. While the CNN model also detects the interference, it shows lower precision with some misclassifications outside the true event period. The CNN-LSTM model presents greater variability, especially near the boundaries of the interference event, indicating less stable predictions. Both U-Time and Encoder models exhibit reduced accuracy, with lower detection probabilities and higher false positive rates in non-interference regions. FCN and Inception perform relatively well, though they have minor misclassifications near the boundaries of the event. The ResNet model shows the weakest performance, with scattered predictions and a higher rate of false positives. Overall, U-TSS outperforms the other models in both detection accuracy and precision for HVDC interference events, while ResNet demonstrates the highest rate of misclassification.

7. Discussion

Even in some complex cases, the U-TSS model still shows excellent detection performance. Figure 13 shows an example of HVDC interference events detection. The X-axis represents the corresponding time of the observation data on that day. The blue curve is the background data after the Z-score standardization, and the red curve is the HVDC events detected mar by after the Z-score standardization. The green and orange curves represent the probability that the U-TSS model predicts as the HVDC and BACKGROUND. Although the duration, direction, amplitude, and shape of each HVDC interference event are different, the U-TSS model can accurately detect all HVDC interference events, and accurately locate the start and end time of each HVDC interference event.

To validate the detection ability of the U-TSS model in actual HVDC interference events, we randomly selected two days of unused geomagnetic field observation data for experimentation. These days are from instrument 1 at station 14014 on May 6, 2023, and instrument 1 at station 42009 on May 28, 2023. We used the trained U-TSS model to detect HVDC interference events.

As shown in Fig. 14, there is only one HVDC interference event marked by the red curve. The U-TSS model successfully detected this HVDC event and accurately identified the start time and end time of the HVDC event.

Figure 15 shows the detection results of the U-TSS model for the data from instrument 1 at station 42009 on May 28, 2023. There are four HVDC interference events on that day, indicated by the red curves and labeled as 1, 2, 3, and 4. The U-TSS model successfully detected events 1 and 3, while events 2 and 4 were not detected correctly. The main reason should be that only HVDC events with a duration of more than 5 minutes were used for training in this paper, so the U-TSS model is not suitable for HVDC events with extremely short duration such as events 2 and 4.



Compared to the existing manual detection technologies for HVDC interference events, the U-TSS model, as a time series segmentation method, presents several significant advantages.

- This model can realize the automatic detection of HVDC interference events, does not rely on the experience of experts, and does not need manual intervention, which can greatly save labor costs.
- It supports the detection of HVDC interference events of different durations, varying amplitude levels, and different directions.
- It can accurately locate the start time and end time of HVDC interference events.
- It exhibits high detection accuracy and strong generalization capability, making it suitable for all stations without requiring separate training or optimization for each station.

Of course, the U-TSS still has some room for improvement, including:

- The recall of the U-TSS model still needs to be further improved, therefore, the network structure of the U-TSS model can be further optimized, such as introducing LSTM or attention mechanism.
- In practical applications, subway, light rail, and HVDC interference events may occur at the same time, which may reduce the accuracy of the U-TSS model.

8. Conclusions

With the proliferation of IoT ces and an increasing reliance on sensor networks for real-time monitoring, the necessity for efficient processing of time series data has become paramount. As the deployment of geomagnetic field observation instruments expands and HVDC transmission lines grow, the cost and complexity associated with the manual detection of HVDC interference events are rising. To address these challenges, this paper introduces U-TSS, a novel time series segmentation model based on the U-net architecture, and apply it to the automatic detection of HVDC interference events in geomagnetic field observation data.

U-TSS employs a fully convolutional sequence-to-sequence architecture to perform dense segmentation on one-dimensional time series data, ensuring precise labeling of each time step, and addressing the challenges posed by complex and lengthy temporal dependencies in IoT-driven applications. By implicitly classifying each time point and aggregating these classifications across varying intervals, U-TSS effectively detects events of different durations, enabling fine-grained segmentation even in the presence of complex temporal patterns. Additionally, the PSO algorithm was employed to optimize U-TSS's hyperparameters, further enhancing its performance. Experiments demonstrate that U-TSS outperforms state-of-the-art

- models with accuracy, precision, recall, F1-score, and AUC values of 95.54%, 88.65%, 76.07%, 0.8188, and 0.9637, respectively, on the test set.
- The key contribution of U-TSS is its ability to accurately segment and detect HVDC interference events in geomagnetic field observation data. This not only significantly reduces the labor cost and time involved in manual detection but also provides an efficient and scalable solution for handling vast amounts of time series data generated by IoT systems. In the future, we plan to extend its application to detect other types of interference events, such as those caused by subways and vehicles.

542 **Funding**

543

544

545546

547

548

549 550

551

552553

554

555 556

557

558

559

560

561

562

563

564 565

566

567

568

569 570

571

572573

This work was supported by the National Natural Science Foundation of China (42164002), the Spark Program of Earthquake Sciences (XH25080C), and the Scientific Research and Development Plan Project of Langfang Science and Technology Bureau (2023011054).

Data availability

The data used in this study were obtained from the geomagnetic network center of China , Institute of Geophysics, China Earthquake Administration, and they can be downloaded at the National Earthquake data Center (https://data.earthquake.cn/). The code of the U-TSS model is available at https://github.com/wangmengyu1/U-TSS.

Declaration of competing interest

The authors declare that they have no known competing financial interests or personal relationships that could have appeared to influence the work reported in this paper.

References

- Abadi M, Barham P, Chen J, Chen Z, Davis A, Dean J, Devin M, Ghemawat S, Irving G, and Isard M. 2016. TensorFlow: a system for Large-Scale machine learning. 12th USENIX symposium on operating systems design and implementation (OSDI 16). p 265-283.
- Acharya UR, Oh SL, Hagiwara Y, Tan JH, Adam M, Gertych A, and San Tan R. 2017. A deep convolutional neural network model to classify heartbeats. *Computers in biology medicine* 89:389-396. 10.1016/j.compbiomed.2017.08.022
- Badrinarayanan V, Kendall A, and Cipolla R. 2017. Segnet: A deep convolutional encoderdecoder architecture for image segmentation. *IEEE transactions on pattern analysis and machine intelligence* 39:2481-2495. 10.1109/tpami.2016.2644615
- Band SS, Janizadeh S, Chandra Pal S, Saha A, Chakrabortty R, Shokri M, and Mosavi A. 2020. Novel ensemble approach of deep learning neural network (DLNN) model and particle swarm optimization (PSO) algorithm for prediction of gully erosion susceptibility. 20:5609. 10.3390/s20195609
- Bao H, Jiang Y, Fan X, Bi X, Bu Y, and Zhang X. 2020. Experitation of the impact of high-voltage direct current transmission on ground electric field observation. *Earthquake Research in China* 36:607-619.
- Chen J, Liu J, Zhang X, and Li S. 2008. Characterization and treatment of geomagnetic disturbance events. Seismological and Geon netic Observation and Research 29:45-49.
- 574 Chen J, Yang D, and Zeng X. 2010. A brief analysis of geomagnetic observation interference overview *Seismological and Geomagnetic Observation and Research* 031:1-5.
- 576 Chen L-C, Papandreou G, Kokkinos I, Murphy K, and Yuille AL. 2017. Deeplab: Semantic image segmentation with deep convolutional nets, atrous convolution, and fully

585

589

590

591

592

593

594

595

596 597

598

599 600

601

602

603

604

605

606

607

608

609

610

611

612

613

614

615 616

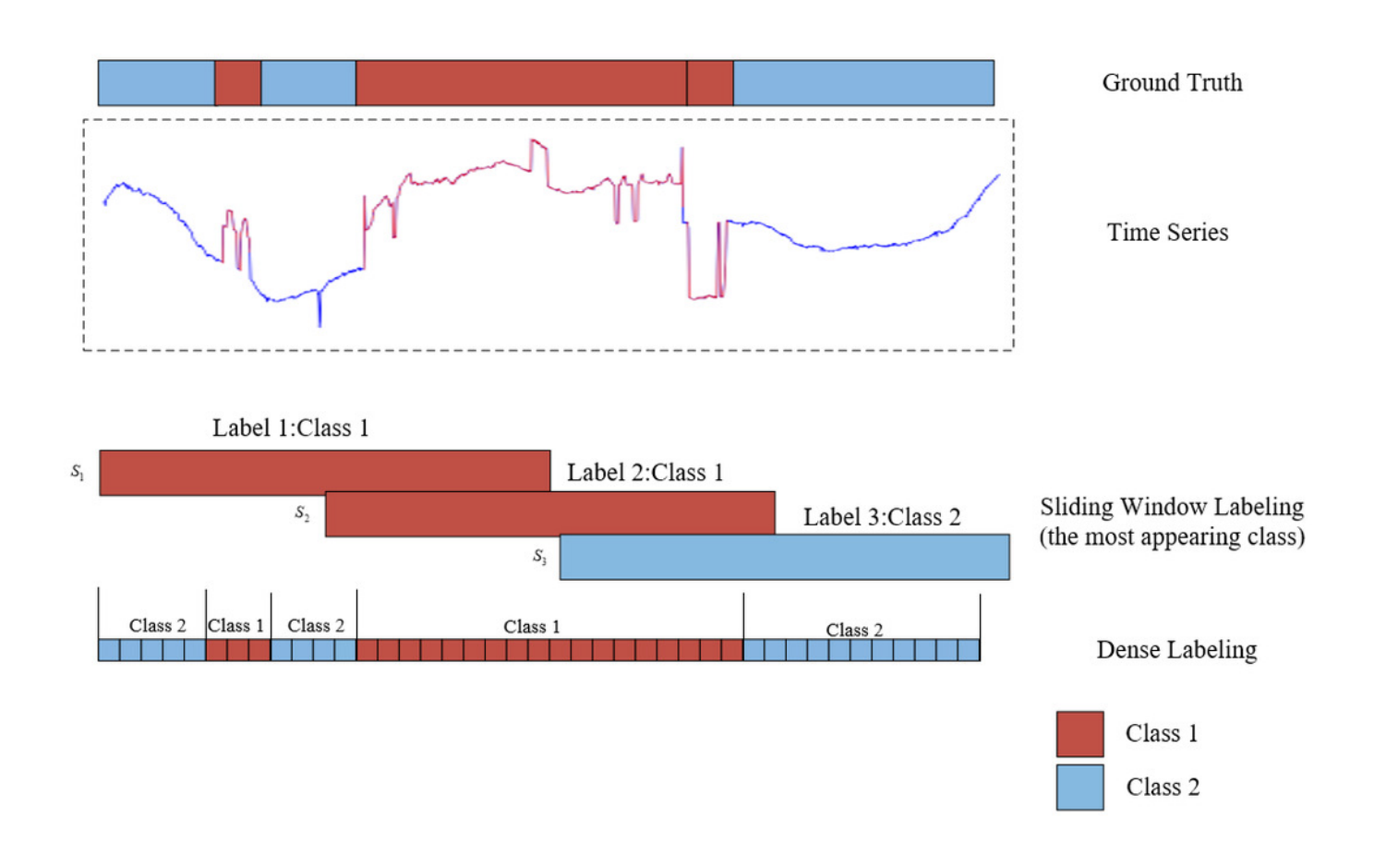
617

- 578 connected crfs. *IEEE transactions on pattern analysis machine intelligence* 40:834-848. 10.1109/TPAMI.2017.2699184
- Chen Z, Tian F, and Sun J. 2016. Overview of key technological advances in geomagnetic navigation research. *Geomatics&Spatial Information Technology* 39:16-18.
- Diederik PK, and Ba J. 2014. Adam: A method for stochastic optimization. 10.48550/arXiv.1412.6980
 - Dua N, Singh SN, and Semwal VB. 2021. Multi-input CNN-GRU based human activity recognition using wearable sensors. *Computing* 103:1461-1478.
- Elmasry W, Akbulut A, and Zaim AH. 2020. Evolving deep learning architectures for network intrusion detection using a double PSO metaheuristic. *Computer Networks* 168:107042. 10.1016/j.comnet.2019.107042
 - Gaugel S, and Reichert M. 2023. PrecTime: A deep learning architecture for precise time series segmentation in industrial manufacturing operations. *Engineering Applications of Artificial Intelligence* 122:106078. 10.1016/j.engappai.2023.106078
 - Gong D, and Yu D. 2000. Three gorges to Changzhou ±500kv high-voltage direct current transmission project introduction. *Electric Power* 33:42-44+53.
 - Ismail Fawaz H, Lucas B, Forestier G, Pelletier C, Schmidt DF, Weber J, Webb GI, Idoumghar L, Muller P-A, and Petitjean F. 2020. Inceptiontime: Finding alexnet for time series classification. *Data Mining Knowledge Discovery* 34:1936-1962. 10.1007/s10618-020-00710-y
 - Jiang Y, and XiuXia Z. 2014. Characterization of the impact of high-voltage direct current transmission on geomagnetic observations. *Earthquake* 34:132-139.
 - Kennedy J, and Eberhart R. 1995. Particle swarm optimization. Proceedings of ICNN'95-international conference on neural networks: ieee. p 1942-1948.
 - Lin X, Qu B, and Fan X. 2020. Characterization of geomagnetic fields H and D disturbed by HVDC transmission. *Chinese Journal of Geophysics* 63:3818-3826.
 - Long J, Shelhamer E, and Darrell T. 2015. Fully convolutional networks for semantic segmentation. Proceedings of the IEEE conference on computer vision and pattern recognition. p 3431-3440.
 - Matias P, Folgado D, Gamboa H, and Carreiro A. 2021. Time series segmentation using neural networks with cross-domain transfer learning. *Electronics* 10:1805. 10.3390/electronics10151805
 - Oh SL, Ng EY, San Tan R, and Acharya UR. 2018. Automated diagnosis of arrhythmia using combination of CNN and LSTM techniques with variable length heart beats. *Computers in biology medicine* 102:278-287. 10.1016/j.compbiomed.2018.06.002
 - Perslev M, Darkner S, Kempfner L, Nikolic M, Jennum PJ, and Igel C. 2021. U-Sleep: resilient high-frequency sleep staging. 4:72. 10.1038/s41746-021-00440-5
 - Perslev M, Jensen M, Darkner S, Jennum PJ, and Igel C. 2019. U-time: A fully convolutional network for time series segmentation applied to sleep staging. *Advances in Neural Information Processing Systems* 32.
- Phan H, Andreotti F, Cooray N, Chén OY, and De Vos M. 2019. SeqSleepNet: end-to-end hierarchical recurrent neural network for sequence-to-sequence automatic sleep staging. *IEEE Transactions on Neural Systems Rehabilitation Engineering* 27:400-410. 10.1109/TNSRE.2019.2896659
- Qolomany B, Maabreh M, Al-Fuqaha A, Gupta A, and Benhaddou D. 2017. Parameters
 optimization of deep learning models using particle swarm optimization. 2017 13th
 International Wireless Communications and Mobile Computing Conference (IWCMC):
 IEEE. p 1285-1290.
- Ronneberger O, Fischer P, and Brox T. 2015. U-net: Convolutional networks for biomedical image segmentation. Medical image computing and computer-assisted intervention—

- MICCAI 2015: 18th international conference, Munich, Germany, October 5-9, 2015, proceedings, part III 18: Springer. p 234-241.
- Serra J, Pascual S, and Karatzoglou A. 2018. Towards a Universal Neural Network Encoder for Time Series. CCIA. p 120-129.
 - Shen H, Zhou J, Zhang X, Feng Z, and Huangpu D. 2005. Analysis of the Impact of HVDC Transmission on Geomagnetic Observations in Jiangsu. *Seismological and Geomagnetic Observation and Research*:65-70.
 - Silva RP, Zarpelão BB, Cano A, and Junior SB. 2021. Time series segmentation based on stationarity analysis to improve new samples prediction. *Sensors* 21:7333. 10.3390/s21217333
 - Supratak A, Dong H, Wu C, and Guo Y. 2017. DeepSleepNet: A model for automatic sleep stage scoring based on raw single-channel EEG. *IEEE Transactions on Neural Systems Rehabilitation Engineering* 25:1998-2008. 10.1109/tnsre.2017.2721116
 - Supratak A, and Guo Y. 2020. TinySleepNet: An efficient deep learning model for sleep stage scoring based on raw single-channel EEG. 2020 42nd Annual International Conference of the IEEE Engineering in Medicine & Biology Society (EMBC): IEEE. p 641-644.
 - Wang M, Gong Q, Chen H, and Gao G. 2023. Optimizing deep transfer networks with fruit fly optimization for accurate diagnosis of diabetic retinopathy. *Applied Soft Computing* 147:110782. 10.1016/j.asoc.2023.110782
 - Wang Z, Yan W, and Oates T. 2017. Time series classification from scratch with deep neural networks: A strong baseline. 2017 International joint conference on neural networks (IJCNN): IEEE. p 1578-1585.
 - Yang X, and Dong H. 2020. Analysis of the impact of high-voltage direct current transmission lines on geomagnetic observations in Gansu and corresponding cour measures. China Earthquake Engineering Journal. p 2.
 - Yin C, Zhang S, Wang J, and Xiong NN. 2020. Anomaly detection based on convolutional recurrent autoencoder for IoT time series. *IEEE Transactions on Systems, Man, Cybernetics: Systems* 52:112-122. 10.1109/TSMC.2020.2968516
 - Yu Y, Mayer T, Knoch E-M, Frey M, and Gauterin F. 2019. Segmentation of Multivariate Time Series with Convolutional Neural Networks. Proceedings of the International Conference on Calibration-Methods and Automotive Data Analytics.
 - Zhang L, Du A, Lang X, Zhang T, Yang D, and Zhao X. 2016. Analysis of daily variation characteristics of geomagnetic field before the Wenchuan earthquake. *Chinese Journal of Geophysics* 59:952-958.
- Zhang L, Yu J, Gao Z, and Ni Q. 2024. A multi-channel hybrid deep learning framework for multi-sensor fusion enabled human activity recognition. *Alexandria Engineering Journal* 91:472-485. 10.1016/j.aej.2024.01.030

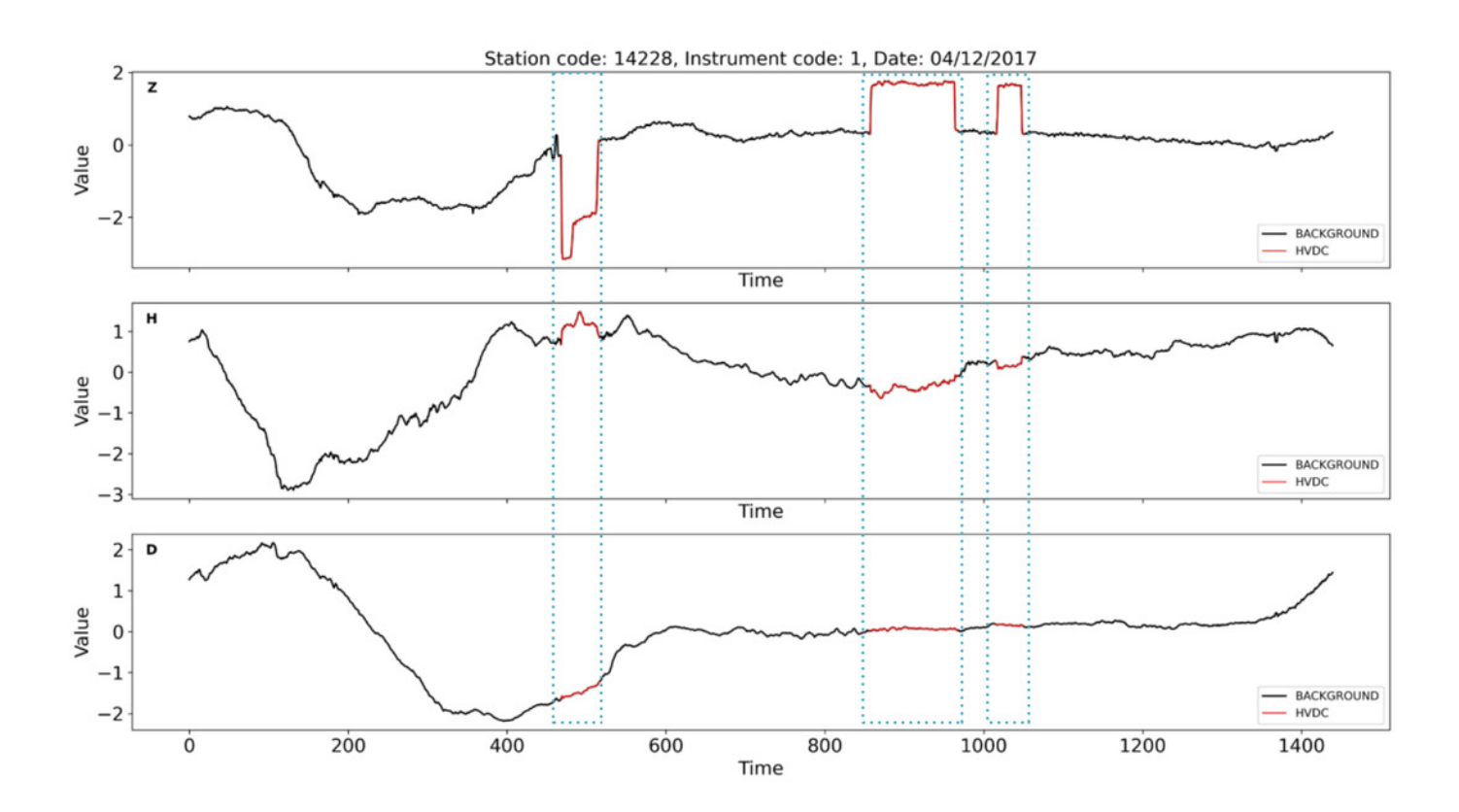
An illustration of the comparative analysis between sliding window labeling and dense labeling for time series segmentation.

The upper section displays a one-dimensional time series data, represented by blue and red curves, along with the corresponding ground truth. The lower section contrasts the two labeling approaches: the sliding window labeling identifies the most frequent class (red) within each window, while the dense labeling assigns labels to every individual time step, providing a detailed representation of the segment classifications.

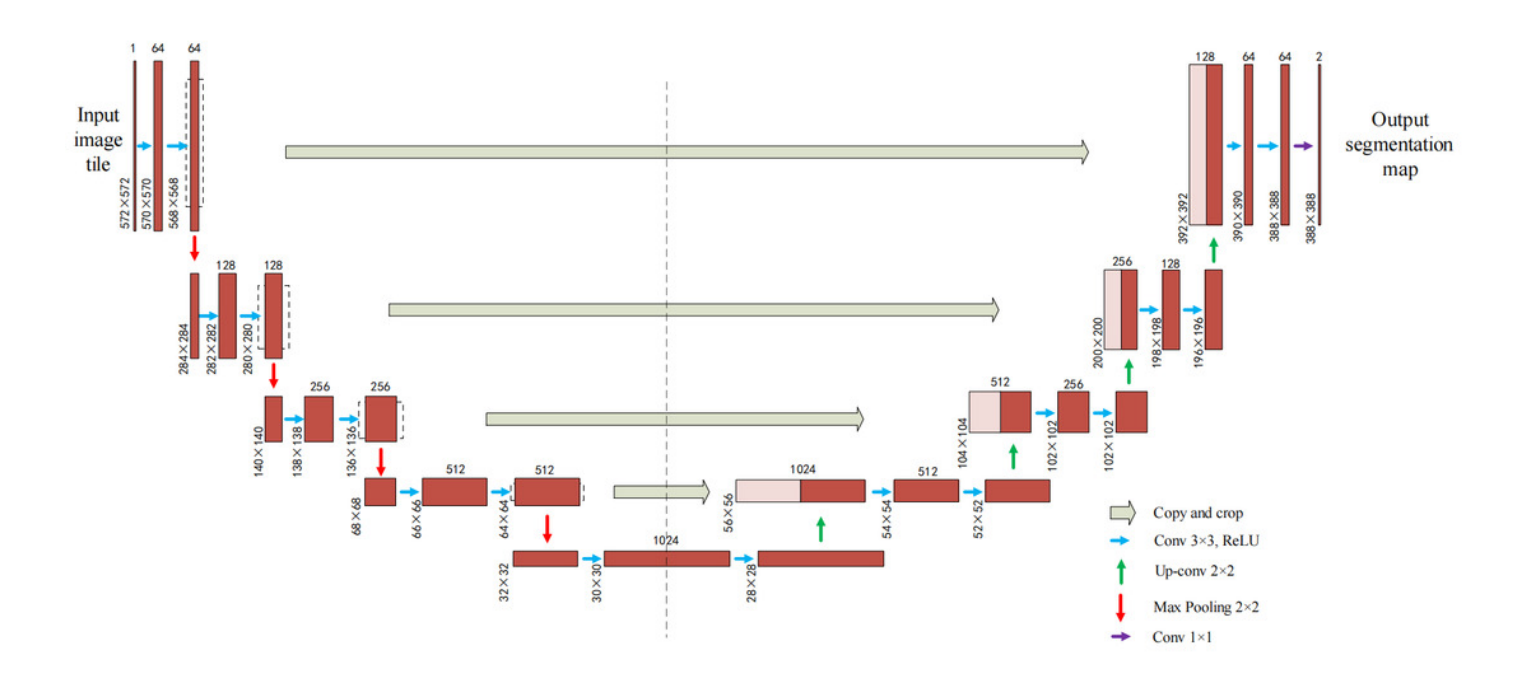


An example of HVDC interference events on instrument 1 at station 14228 on April 12th, 2017.

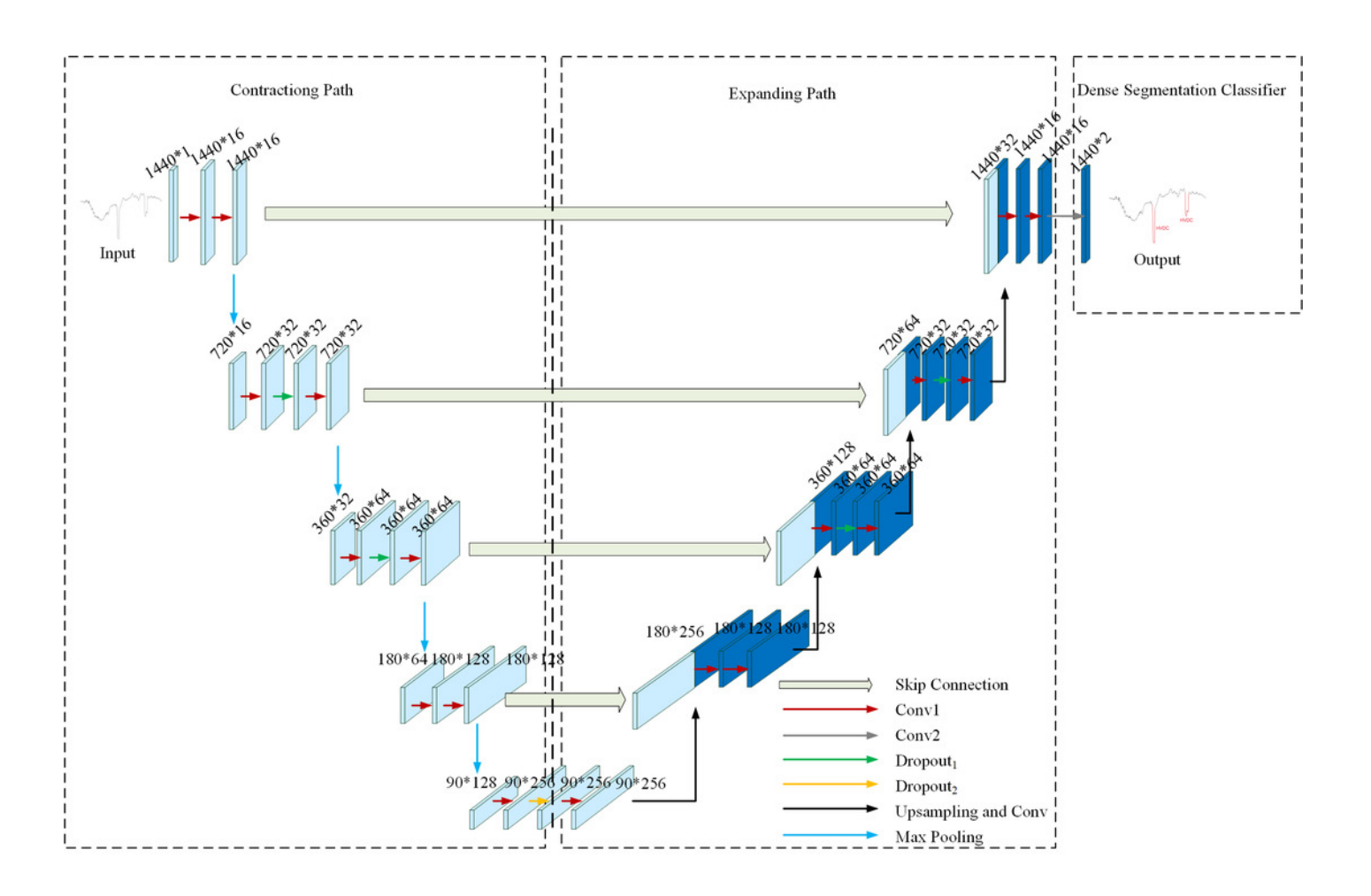
The red curve marked with a dotted box represents HVDC interference events. The Z-component is significantly affected by HVDC interference events, while the D and H components show no impact.



The network architecture of the U-Net model.

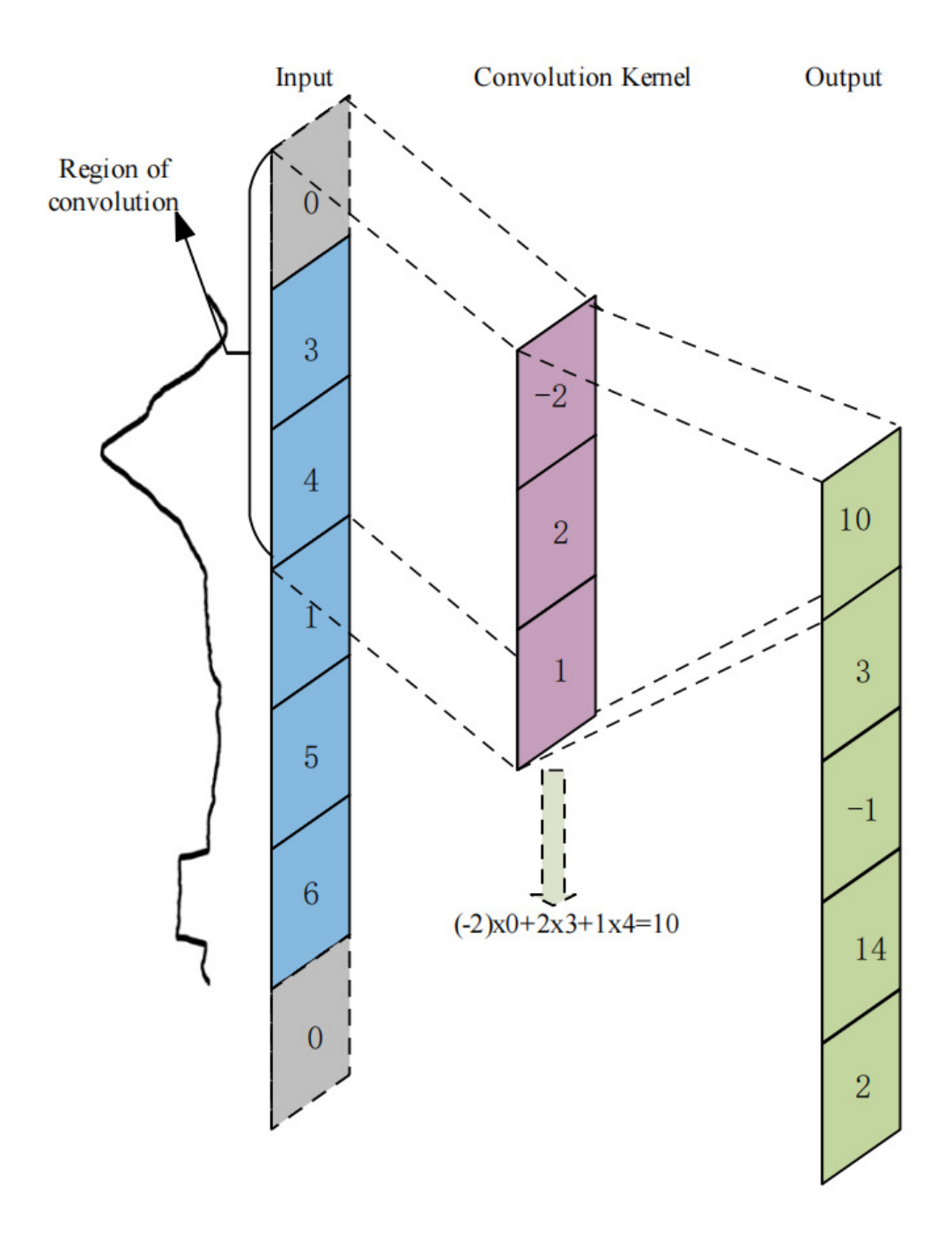


The network structure of the U-TSS model.

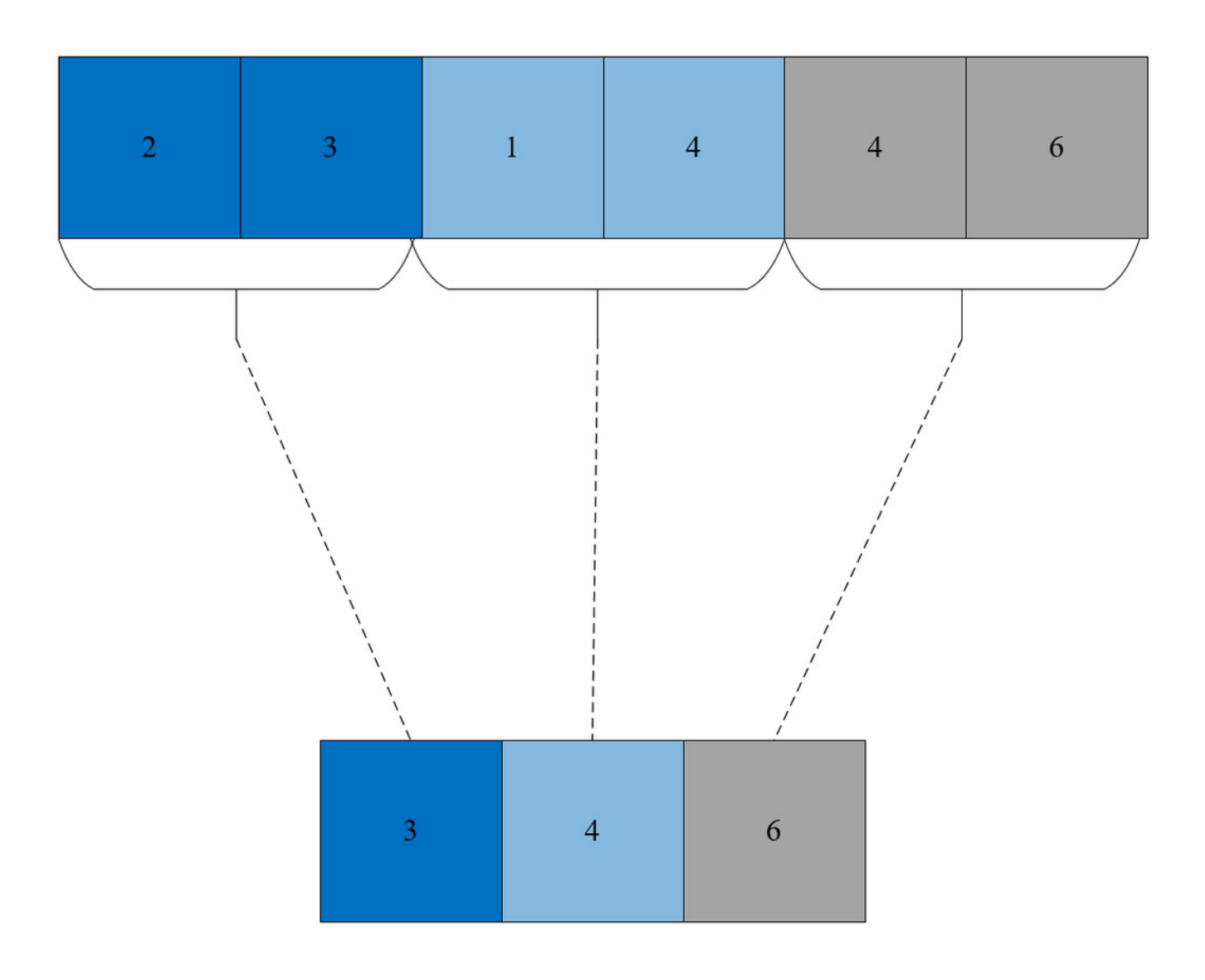


An example of 1- dimensional convolutional operation.

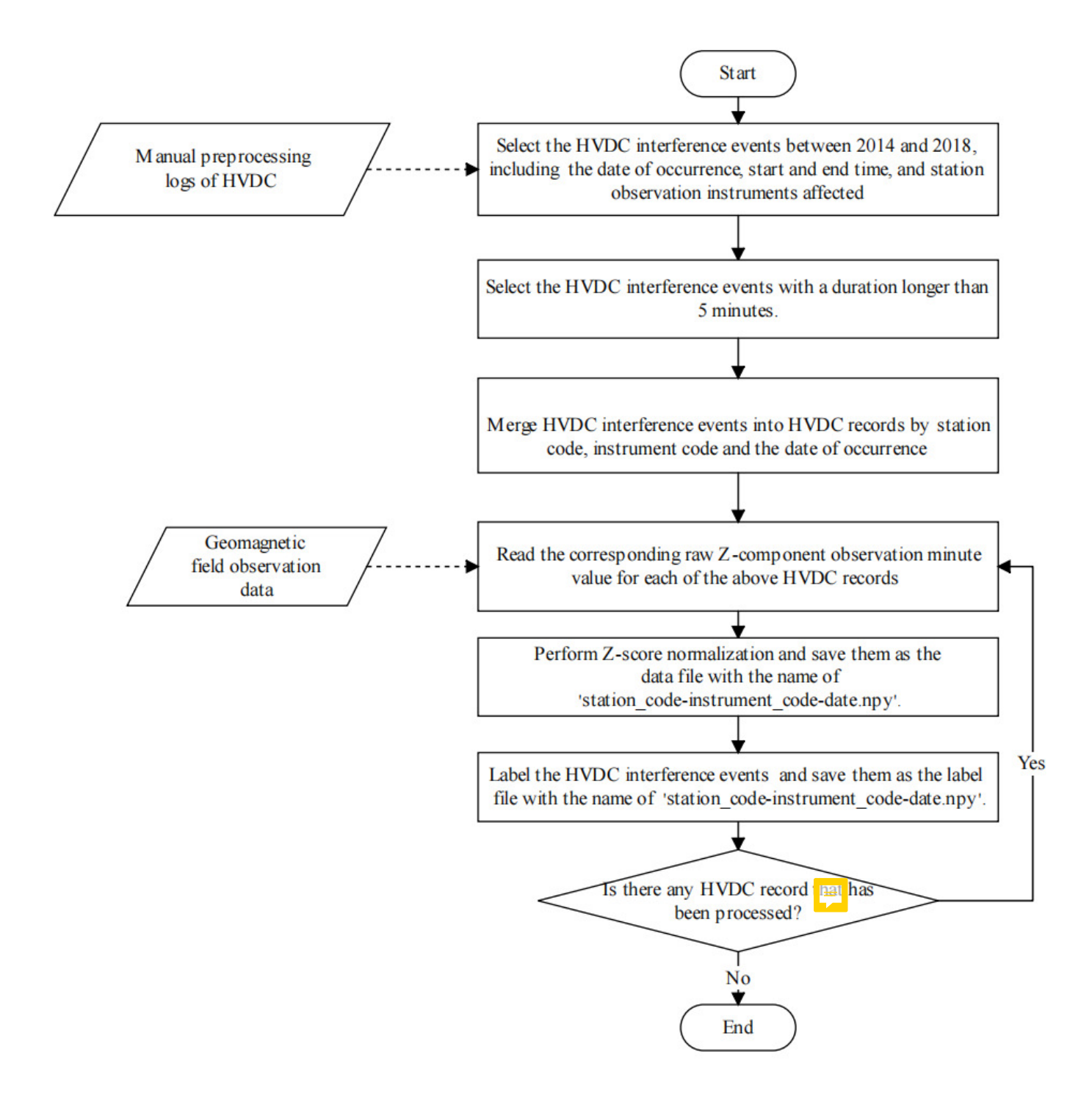
The blue region on the left side represents the input feature map, where the time point values selected by the curly brace are the elements participating in the first convolutional operation. The gray region represents the padding time points. The pink region represents the 1-dimensional convolution kernel in a time series, which slides along the input feature map, performs dot-multiplication operations with the values at corresponding positions, and sums them up to end up with the green region on the right, the output feature map.



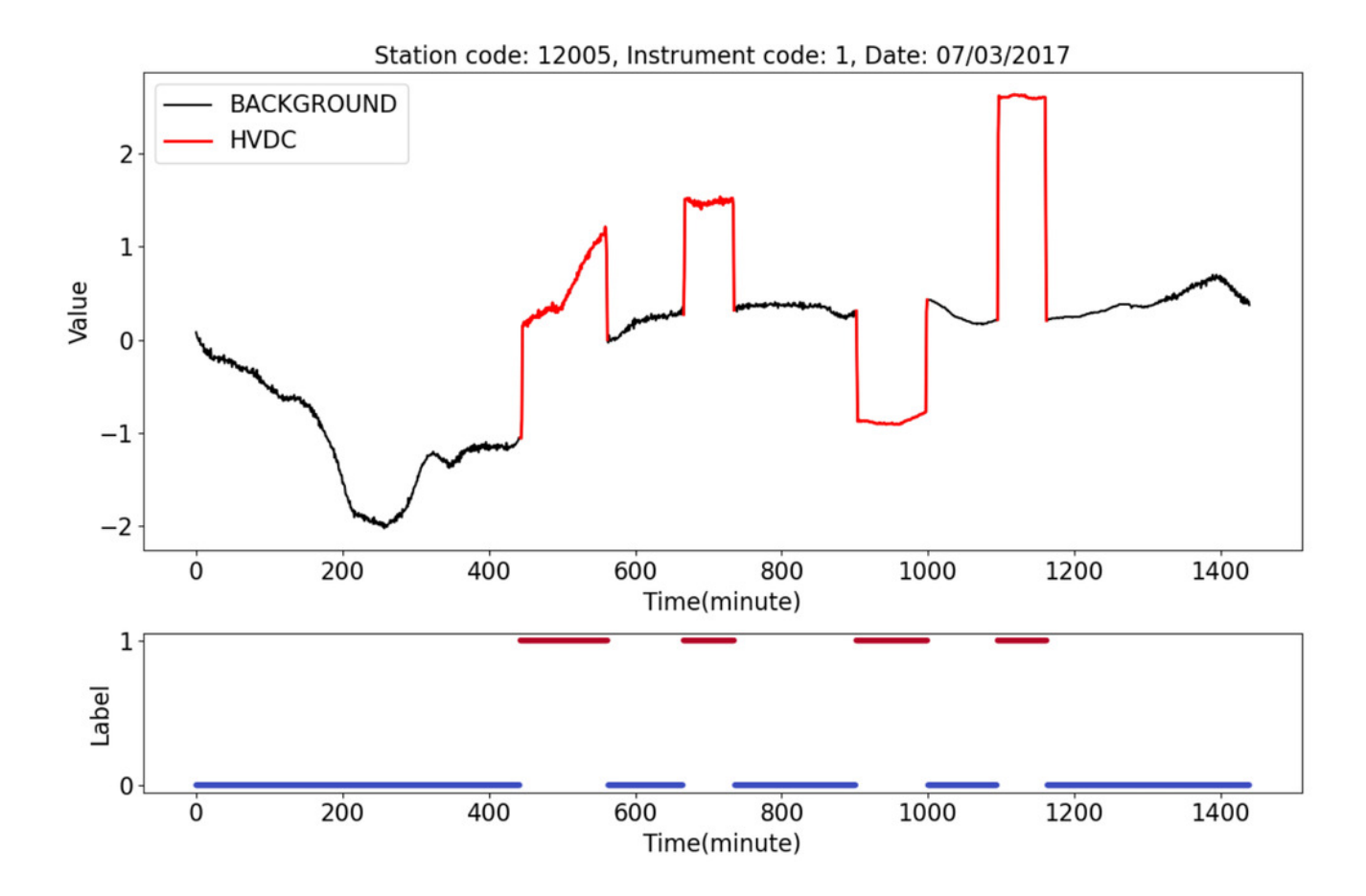
An example of 1-dimensional max pooling.



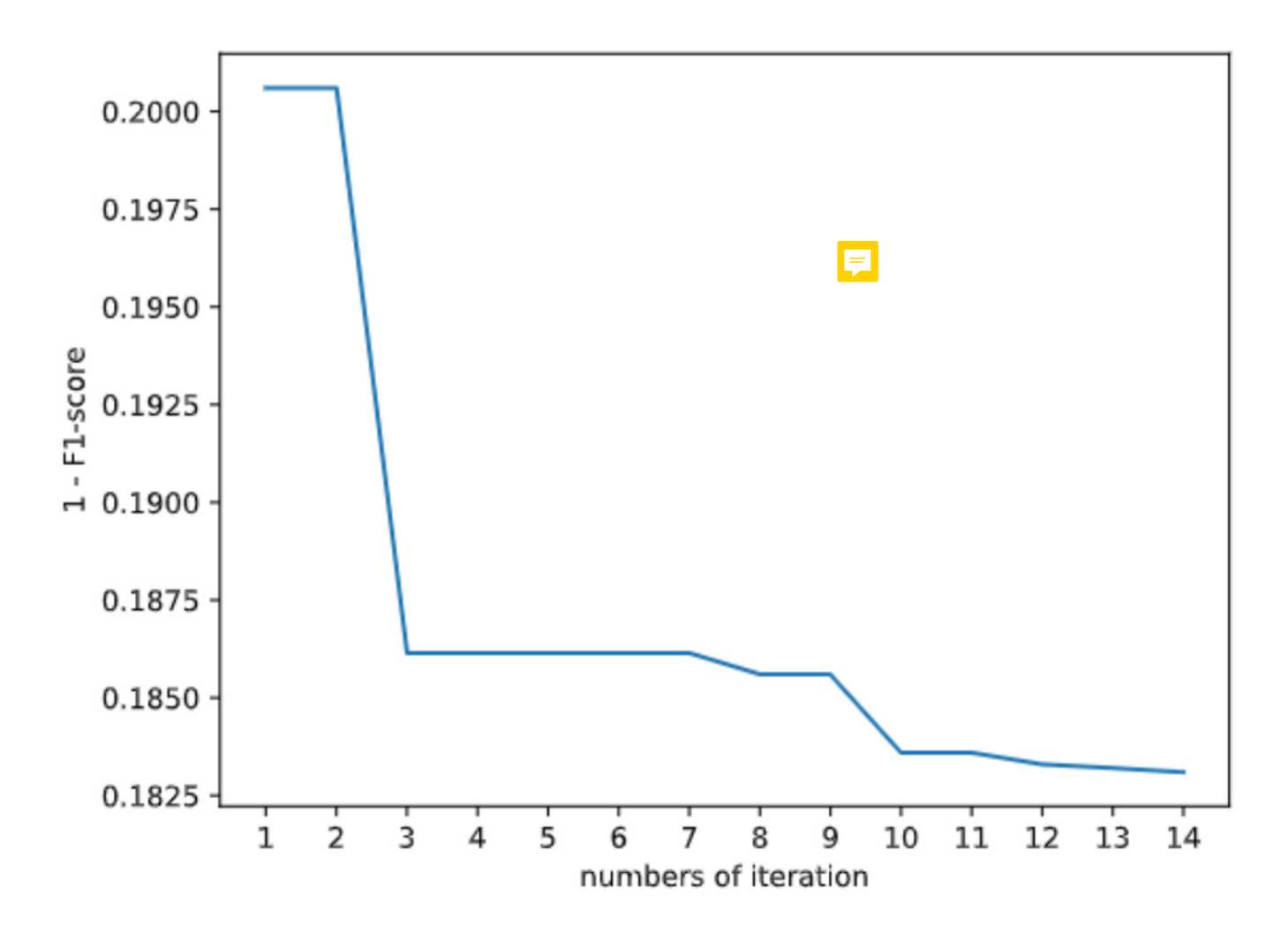
The flowchart of the HVDC sample production process.



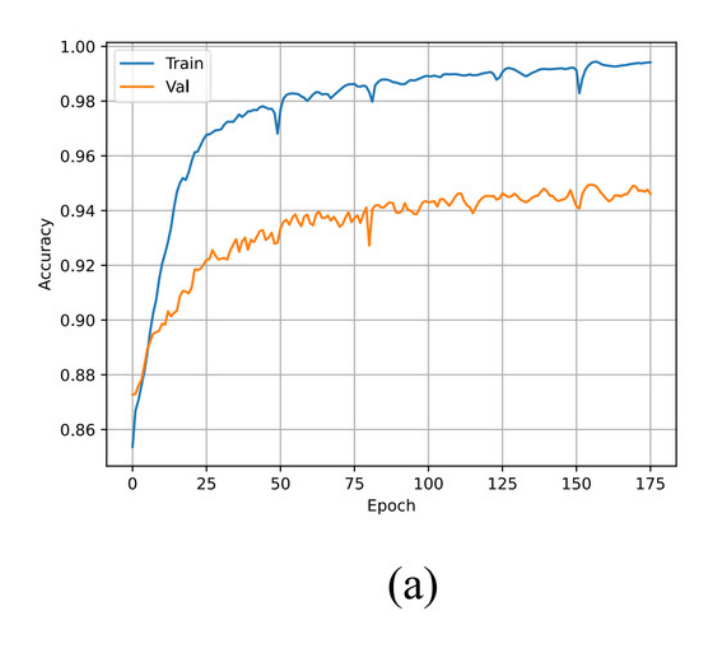
An example of HVDC sample.

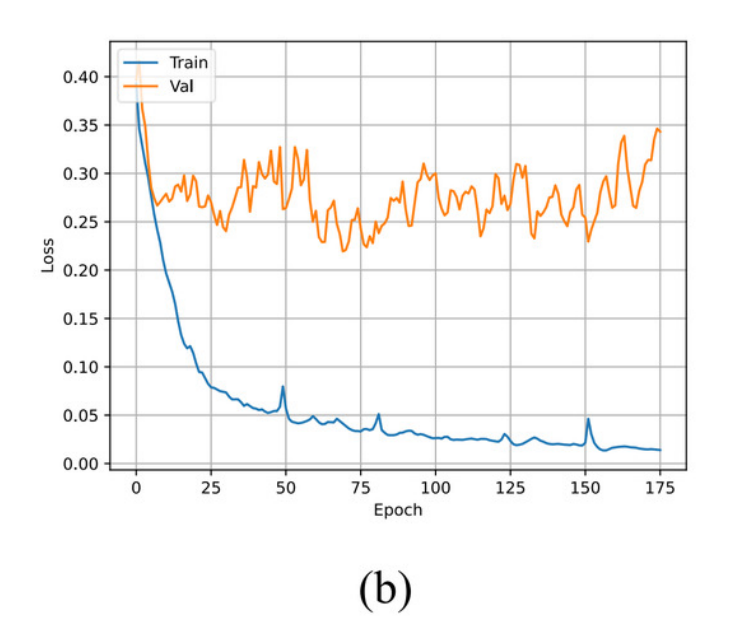


The fitness curve of the PSO algorithm.

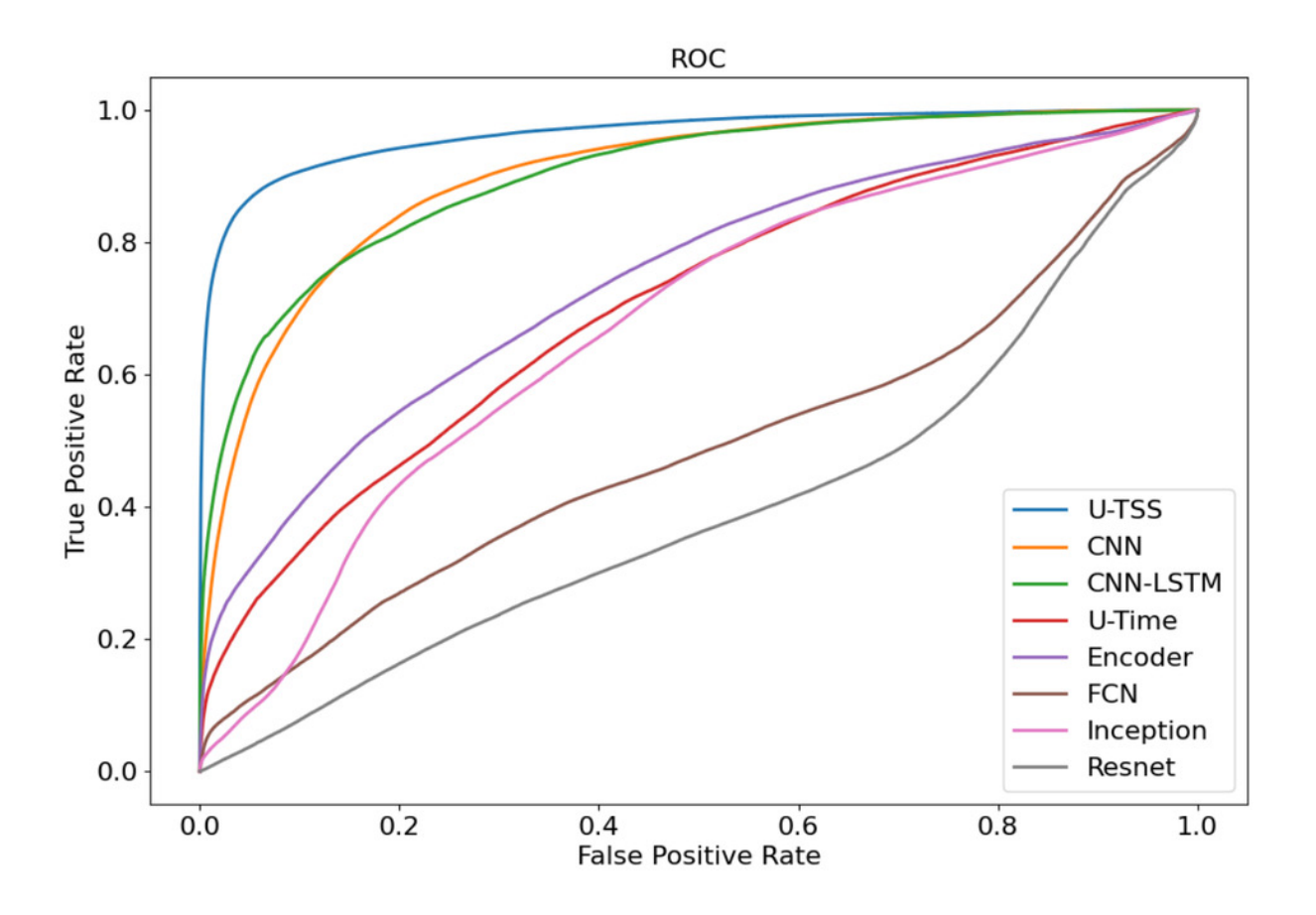


The accuracy and loss curves of the U-TSS: (a) The accuracy curve; (b) The loss curve.

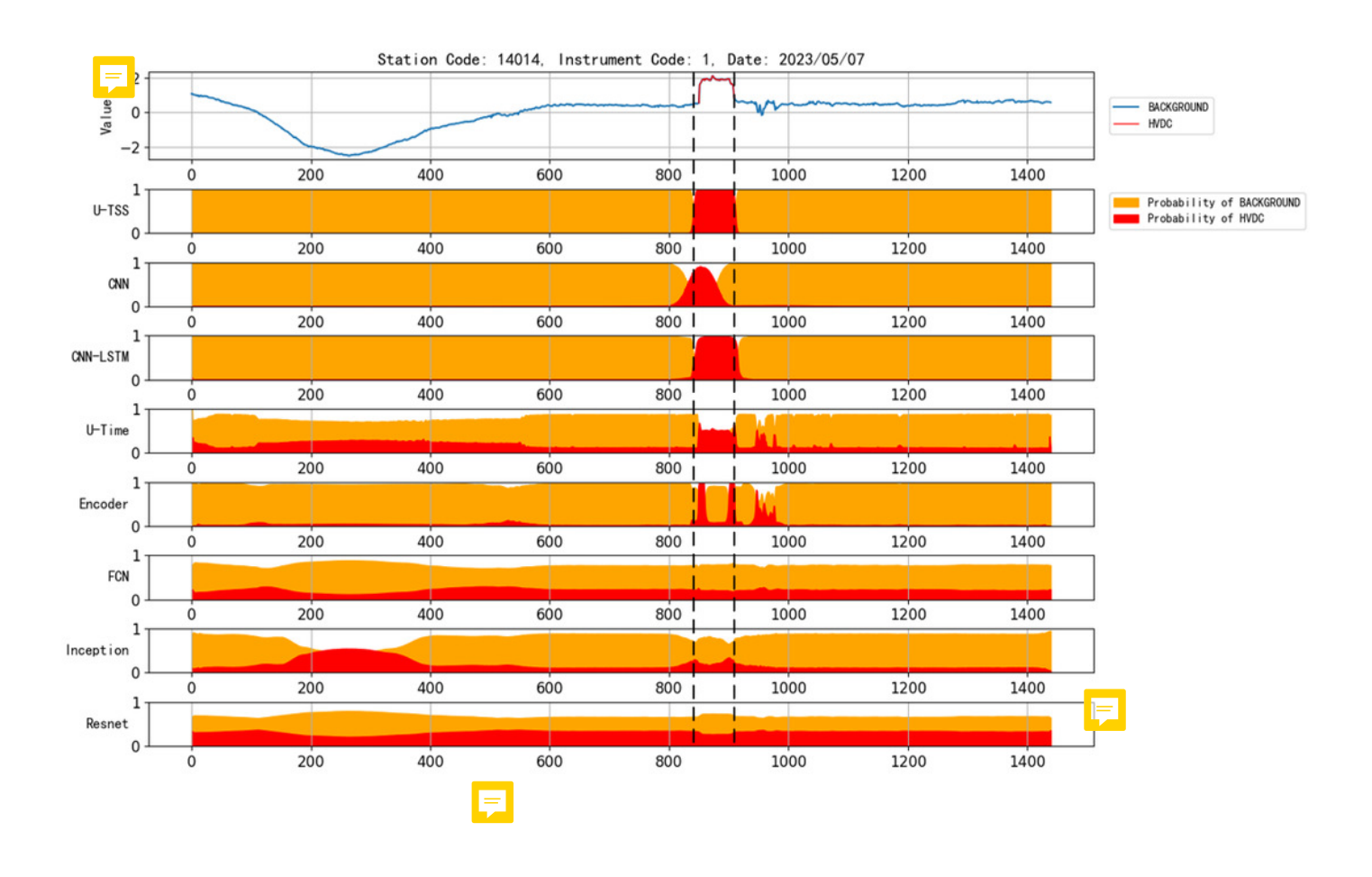




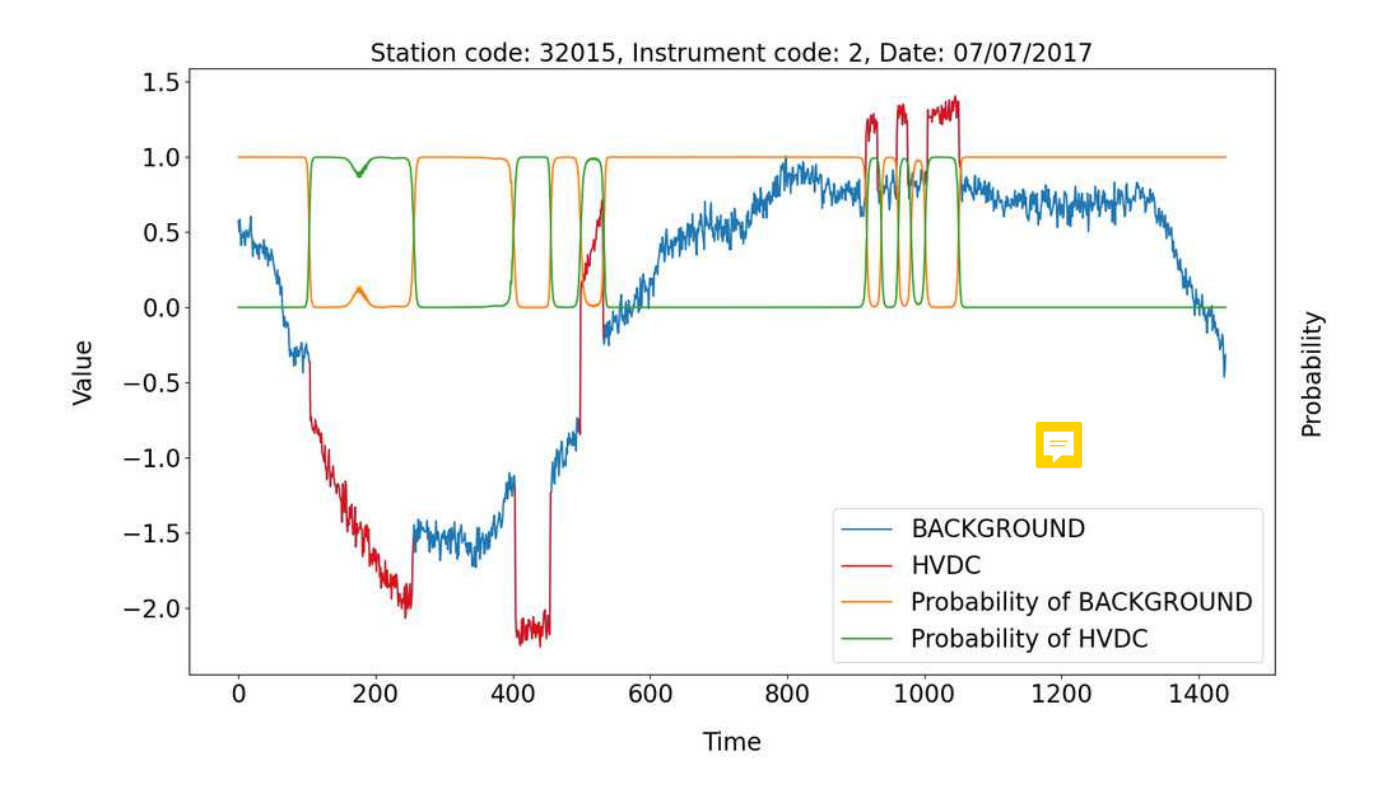
The ROC curves of different models.



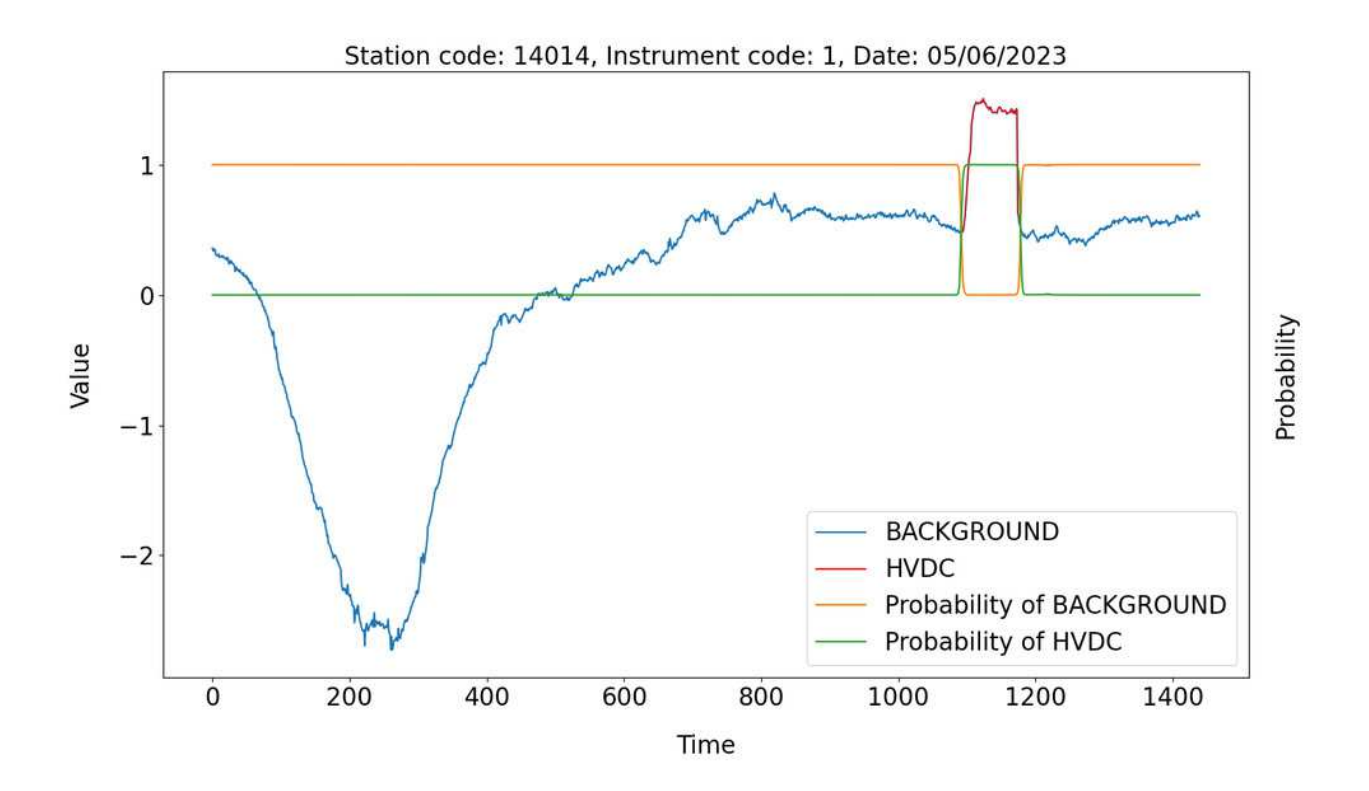
Comparison of the performance of various models for detecting HVDC interference events in geomagnetic field data.



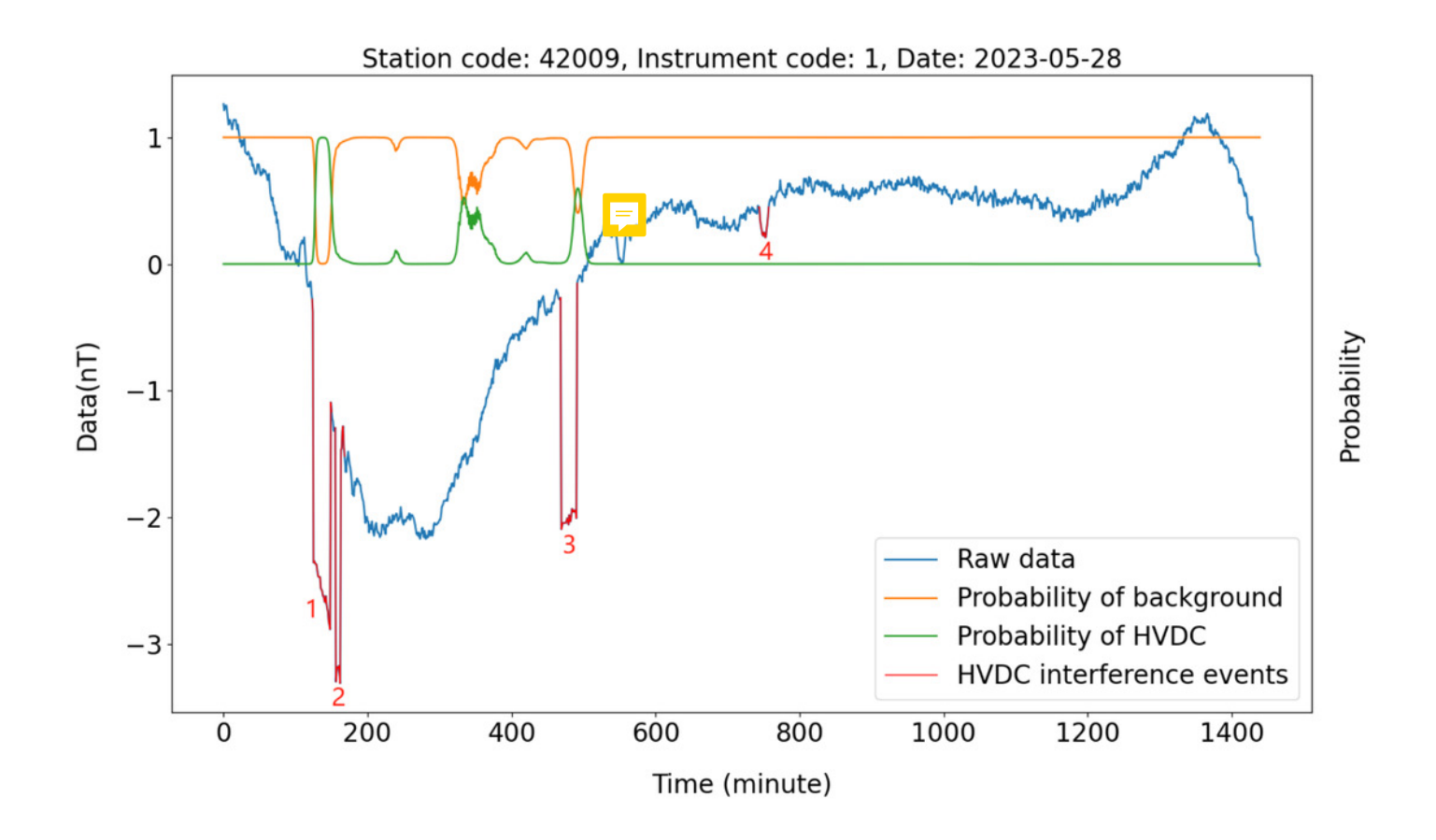
An example of the detection result of the U-TSS.



The detection results of the U-TSS model for the data from instrument 1 at the station 14014 on May 6, 2023.



The detection results of the U-TSS model for the data from instrument 1 at the station 42009 on May 28, 2023.



Manuscript to be reviewed

Table 1(on next page)

Confusion matrix.

Prediction Actual	1 (HVDC)	0(BACKGROUND)
1 (HVDC)	TP	FN
0(BACKGROUND)	FP	TN

Manuscript to be reviewed

Table 2(on next page)

The parameters settings to be optimized in PSO.

Manuscript to be reviewed



Kernel Size range	Learning rate range	Dropout ₁ range	Dropout ₂ range
16 to 128	0.000001 to 0.01	0 to 0.6	0 to 0.6

1

Manuscript to be reviewed

Table 3(on next page)

Experimental results of different models on the test set.

EvaluationMetrics Method	Accuracy	Precision	Recall	F1-Score	AUC
U-TSS	95.54%	88.65%	76.07%	0.8188	0.9637
CNN	90.03%	70.19%	43.13%	0.5343	0.8995
CNN-LSTM	91.21%	75.45%	49.99%	0.6013	0.7405
TinySleepNet	90.11%	83.98%	68.00%	0.7257	-
U-Time	86.22%	29.52%	32.99%	0.3116	0.7130
Encoder	87.99%	85.71%	11.37%	0.2007	0.4870
FCN	86.74%	63.06%	0.14%	0.0027	0.6706
Inception	85.03%	23.91%	5.90%	0.0946	0.3968
Resnet	86.76%	56.67%	0.90%	0.0177	0.8985